Applying Green Chemistry to the Photochemical Route to Artemisinin

Zacharias Amara,[1] Jessica F. B. Bellamy,[1] Raphael Horvath,[1] Samuel J. Miller,[1] Andrew Beeby,[2] Andreas Burgard,[3] Kai Rossen,*[3] Martyn Poliakoff*[1] and Michael W. George*[1]

[1] School of Chemistry, University of Nottingham, University Park, Nottingham, NG7 2RD, UK.

[2] Department of Chemistry, University of Durham, South Rd, Durham DH1 3LE, UK.

[3] Sanofi-Aventis Deutschland GMBH, C&BD Frankfurt Chemistry, Process Research, Industriepark Hoechst. D-65926 Frankfurt am Main, Germany.

* Corresponding authors: e mail Kai.Rossen@sanofi.com, Martyn.Poliakoff@nottingham.ac.uk, Mike.George@nottingham.ac.uk

Artemisinin is an important antimalarial drug but, currently, the environmental and economic costs of its semi-synthetic production are relatively high. Most of these costs originate in the final chemical steps which follow a complex acid- and photo-catalysed route with oxygenation by both singlet and triplet oxygen. We demonstrate that applying the principles of green chemistry can lead to innovative strategies which avoid many of the problems in current photochemical processes. The first strategy combines the use of liquid CO_2 as solvent and a dual-function solid acid/photocatalyst. The second is an ambient temperature reaction in aqueous mixtures of organic solvents; the only inputs are dihydroartemisinic acid, O_2, and light — the output is pure, crystalline artemisinin. Everything else — solvents, photocatalyst and aqueous acid — can be recycled. Some aspects developed here through green chemistry are likely to have wider application in photochemistry and other reactions.

The principles of green chemistry[1,2] are a checklist of metrics for judging the environmental cost and efficiency of a given chemical reaction or process. These principles include minimization of waste, avoidance of toxic solvents and reagents, elimination of unnecessary steps and minimization of energy usage. Their application has been particularly effective in pharmaceutical manufacture, not least because those processes often involve many steps, each of which may involve toxic compounds and generate waste. For example, in the case of Viagra, application of these principles has led to a huge reduction in solvent usage.[3] Green chemistry principles often lead to simplified and cost effective strategies which, as we demonstrate here, can open up new processing opportunities.

Minimizing the financial and environmental costs of manufacturing artemisinin (**1**) is a major goal for supplying this antimalarial drug at a price that would permit its even wider use in economically developing parts of the world.[4,5] The current supply of **1** obtained by extraction from *Artemisia annua* does not always meet demand. Therefore, supplementing this with a semi-synthetic manufacturing process from more abundant biosynthetic precursors is a promising way forward.[6] Photochemical generation of singlet oxygen, $^1O_2$, is a key step in the only commercially viable route for the semi-synthetic production of **1**. It begins with a biosynthetic step,[7] namely the use of genetically modified yeast to convert glucose to artemisinic acid, **2**, which is then hydrogenated diastereoselectively to **3** (Fig. 1).[8-10] With the carbon skeleton already assembled, the final conversion of **3** to **1** formally requires the introduction of two O_2 molecules. In this context, photochemically generated $^1O_2$ is attractive from a green chemistry point of view because (a) both of the oxygen atoms are incorporated

into the product, avoiding waste and (b) photochemical energy is delivered selectively unlike thermal reactions, which require the heating of the entire reaction mixture.

In the industrial process currently implemented at Sanofi, the oxygenation is preceded by an additional step, the esterification of **3** to a mixed anhydride.[10] However, the direct Schenck ene oxidation of **3** with photochemically generated $^1O_2$ is also possible, as first described by Acton and Roth[11,12] and more recently by Seeberger and coworkers in an elegant continuous process.[13,14] This can lead several possible regioisomeric hydroperoxides, only one of which, **4**, can be transformed into **1** (see ESI, Scheme S1). The only other isomer generated in any reasonable quantity is **5** and the ratio of **4**:**5** has been shown to be highly temperature dependent in a range of solvents,[10,13-15] with low temperatures favoring the formation of **4**. The resulting hydroperoxide **4** is then converted to **1** in an acid-catalyzed rearrangement followed by a second oxygenation, a sequence studied in some detail by Brown and co-workers.[15,16]

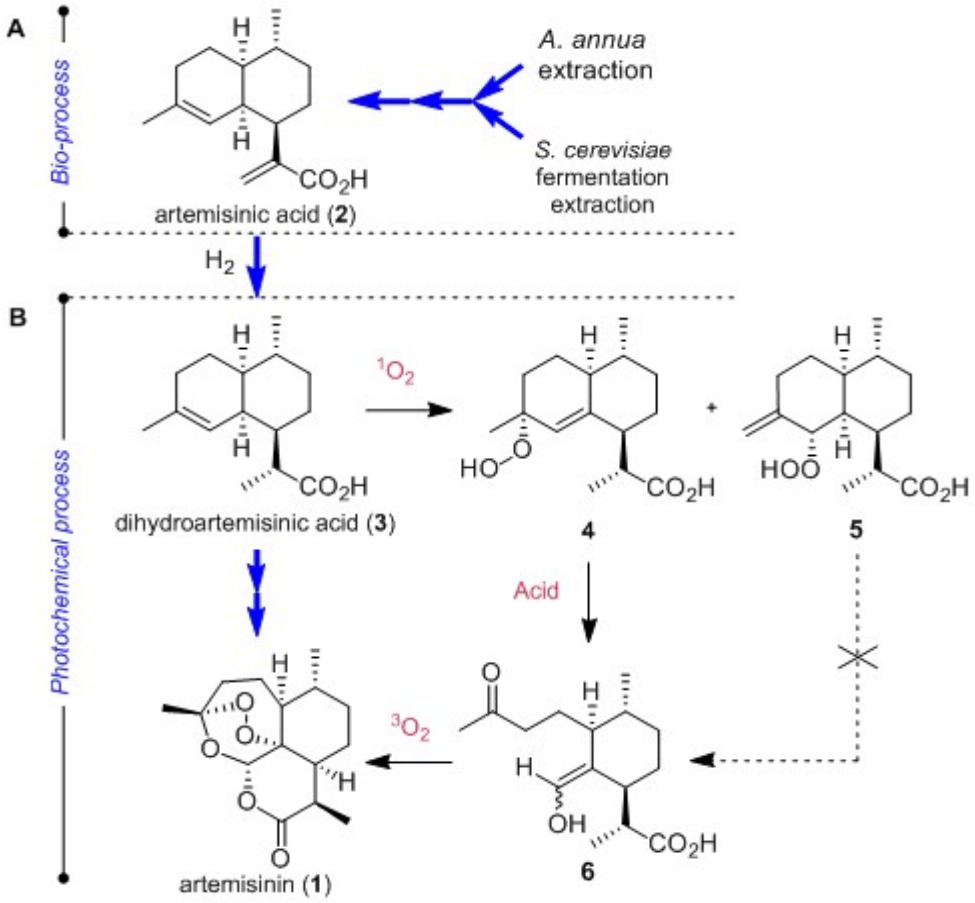

Fig. 1. Semi-synthetic production of the potent anti-malarial artemisinin, **1.** (**A**) Initial production of artemisinic acid (**2**) either by extraction from *Artemisia annua* or by a fed-batch fermentation processes (*Saccharomyces cerevisiae*). (**B**) Chemical conversion of **2** to **1** by hydrogenation to **3** followed by photo- and acid-catalysis. **5** is the predominant unwanted hydroperoxide, formed during reaction of **3** with $^1O_2$. The current Sanofi process adds an extra activation step to form the ester of **3** (mixed anhydride) rather than the free acid.[10] Hydroperoxide **4** is converted through an acid-catalyzed ring opening process into enol **6** (**6** has been observed under oxygen free conditions). This reactive intermediate is then finally oxidized into **1**, a step which requires heating to room temperature and longer reaction times.

The current industrial process and all of the published work mimic the biosynthetic route to **1** in a genuinely atom economical way. Most variations of this route give between 50% and 60% yield of **1** after optimization (55% for the industrial process) which appears an inherent

limitation of the chemistry rather than a function of the particular process. Nevertheless, these approaches fail to tackle a number of key green chemistry issues. These begin with the use chlorinated solvents such as dichloromethane (DCM) for the $^1O_2$ reaction; the use of the relatively toxic acid, trifluoroacetic acid (TFA); the need to carry out the photo-oxidation at low temperature (typically -20°C) to increase selectivity towards **4**;[13-15] and the ultimate purification of **1**, involving multiple washings to remove the acid, the loss of photosensitizer and solvent exchange to allow crystallization.[10] In addition, all of these processes generate **1** in the presence of free acid which is concerning because **1** is not stable under acidic conditions[17] and this could ultimately reduce productivity.

Here we outline two separate and different strategies, based on principles of green chemistry, which circumvent most of these problems. These strategies are (i) the use of liquid CO_2 as the reaction solvent, using a potentially recyclable heterogeneous photosensitizer/acid system as shown in Fig 2 and (ii) the use of recyclable aqueous mixtures containing water soluble acid- and photo-catalysts, see Fig 3. Below, we describe these approaches in more detail and then compare them in terms of "green metrics" and their possible impact on the environmental cost of production of **1**.

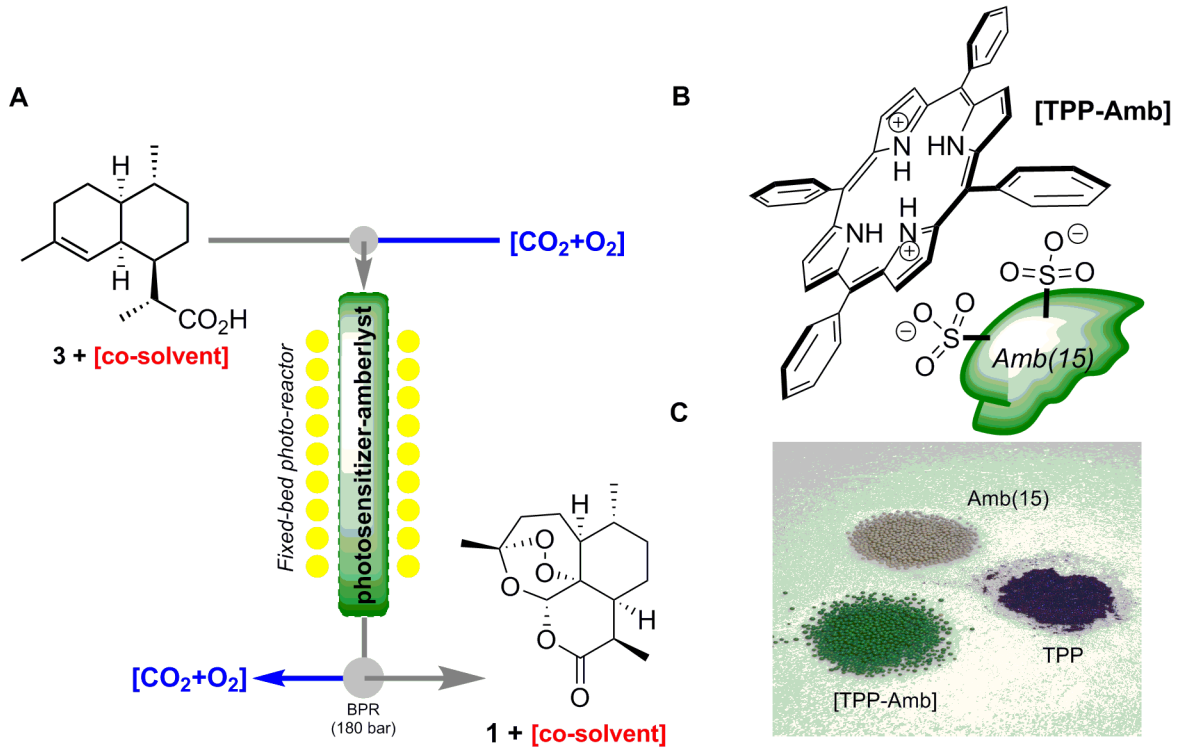

Fig. 2. Our first strategy, the one-pot semi-synthesis of artemisinin in *liquid* CO_2 with a dual function heterogeneous catalyst. (**A**) Schematic of the continuous flow reactor; it consists of a transparent sapphire tube containing the immobilized photocatalyst, surrounded by a concentric transparent cooling jacket and three banks of high power white light emitting diodes (LEDs, see the ESI for a fuller description). As **3** is a solid, a co-solvent is required to enable pumping into the reactor. (**B**) Schematic of the catalyst, consisting of porphyrin photosensitizer bound to Amberlyst-15. While similar work has been carried out to immobilize porphyrins and phthalocyanins by a number of groups,[27-30] using covalent linkages,[29,30] electrostatics,[28] and embedding,[28] we believe that in this case it is the basicity of the porphyrin that enables anchoring through di-protonation of the porphyrin core.[31] (**C**) Photograph showing the difference in color between the free and the supported porphyrins and Amberlyst 15.

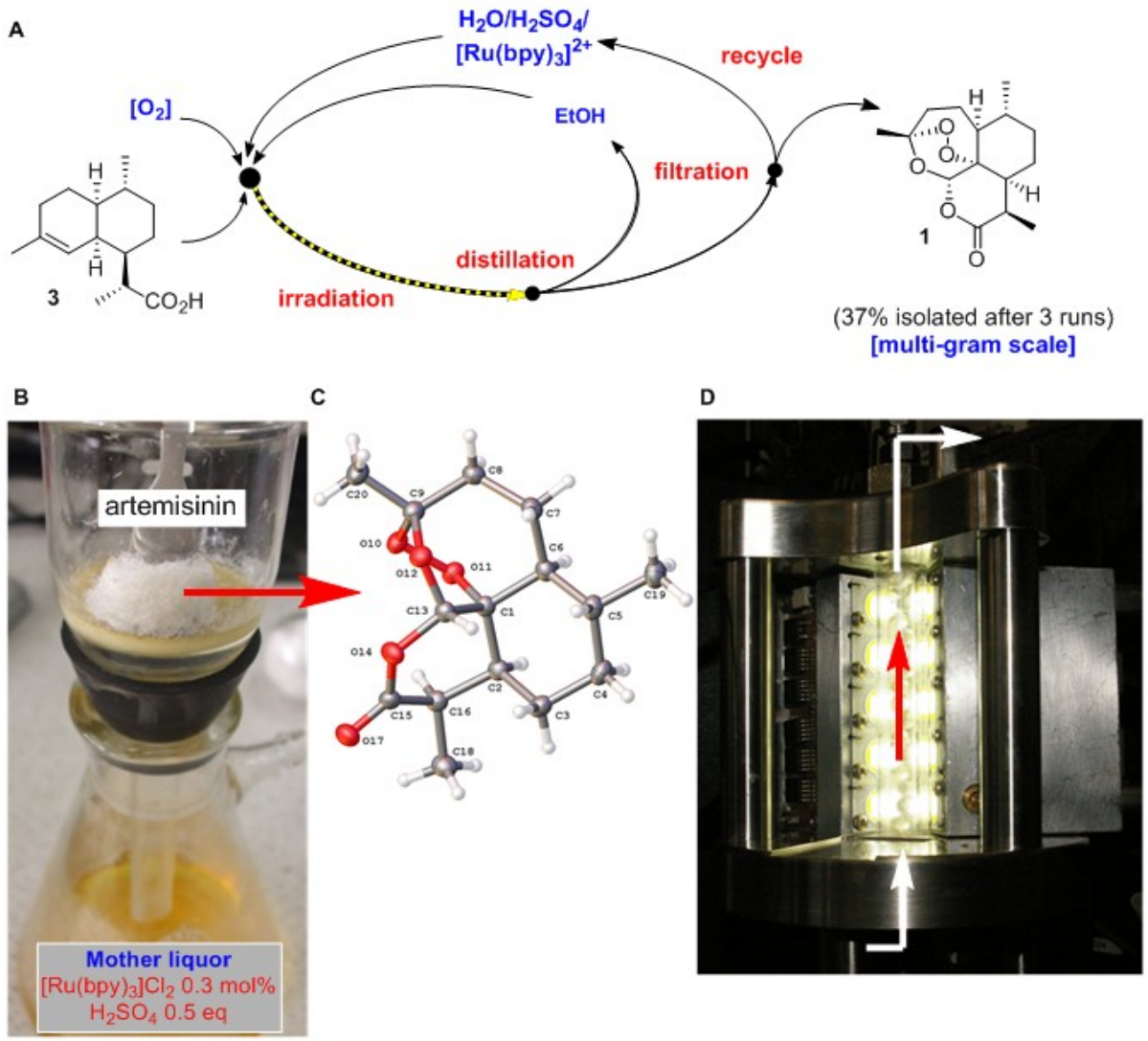

Fig. 3: Our second strategy, photocatalytic oxygenation of **3** dissolved in EtOH + H_2O, (**A**) Schematic of the non-optimized process illustrating how **1** can be recovered from the solution by partial evaporation of the EtOH to reduce the solubility of **1** in the aqueous solvent. (**B**) Photograph taken at the filtration stage, showing crystals of **1**. (**C**) Single crystal X-ray structure obtained from a crystal removed directly from the crude solid without any further re-crystallization. (**D**) Photograph of the high pressure photo-reactor modified for upward flow of aqueous mixtures, showing the sapphire tube filled with glass balls and surrounded by LEDs.

Strategy 1: Dual-functional heterogeneous photocatalysis in liquid CO_2

CO_2 is an attractive solvent for greener chemistry because it is cheap, renewable and non-toxic. For reactions of $^1O_2$, it has the benefit of being non-flammable and the lifetime of $^1O_2$ is relatively long,[18] which is of key concern when selecting a suitable solvent for photo-oxidation reactions. In addition, supercritical CO_2 ($scCO_2$) has been shown to be a useful solvent for reactions involving permanent gases (e.g. H_2, CO or O_2) as they are completely miscible with $scCO_2$.[19-21] Our group recently demonstrated that the reactions of $^1O_2$ can be carried out efficiently in a continuous flow reactor in $scCO_2$ with either homogeneous or immobilized porphyrin photocatalysts.[22-26] We have now applied this approach to the reaction of $^1O_2$ with **3** at low temperature, taking CO_2 into the *liquid* phase, with an added advantage for scale-up since the vapour pressure of liquid CO_2 is much lower than for $scCO_2$, thereby reducing the pressure requirements for future reactors. Until now, *liquid* CO_2 has rarely been used as a solvent

because most reactions carried out in CO_2 have been *thermally* initiated which almost immediately raises CO_2 above its critical temperature, 31 ^oC.

As shown in Fig 2, we have used an immobilized porphyrin in order to remove the need to separate the photocatalyst from the product. In the past, porphyrin immobilization has most often been carried out through covalent bonding but this involves multiple low yielding steps to modify the photocatalyst and tedious work up procedures.[23] We have developed a simple method that enables straightforward anchoring of *meso*-tetraphenylporphyrin (TPP) or *meso*-tetrakis(pentafluorophenyl)porphyrin (TPFPP), both of which are commercially available, porphyrins onto the sulfonated cross-linked polystyrene ion-exchange resin, Amberlyst-15 (Amb), see Fig. 2 and ESI. This gives a *dual catalyst* with both the Brønsted acidic and photo-catalytic functions needed to convert **3** to **1**.

A number of different conditions were investigated with TPP-Amb which appears to be the more robust bifunctional system with negligible leaching (entry 3 and ESI Table S1); these results are comparable to the use of a *homogeneous* system, using TPFPP and *2*-mesitylene sulfonic acid, both of which are soluble in liquid and $scCO_2$ (see ESI). Full conversion was achieved after four passes at 0.12 $mL.min^{-1}$ (entry 3). Interestingly, doubling the length of the photoreactor resulted in near 100% conversion of **3** in a single pass at the same flow rate (entry 4). The conditions were not fully optimized but nevertheless yields ca. 50% were obtained (entries 3 & 4), comparable to published routes.[9,13] Most yields were measured directly from NMR of the product solution but some samples of **1** were isolated and more fully characterized by a variety of techniques including NMR, melting point and optical rotation; the data are in excellent agreement with those recorded from an authentic sample of **1** from the commercial process (see ESI).

As with previously reported batch reactions,[15] it was found that acid must be present at the photo-oxidation step to minimise the formation of by-products arising from elimination of H_2O_2 from **4**. The bifunctional nature of the TPP-Amb/CO_2 system therefore has the advantage that **4** is no longer accumulated in the reaction medium and undergoes Hock rearrangement more selectively. In addition, combining the use of CO_2 and these bifunctional heterogeneous catalysts enables **1** to be obtained directly at the outlet of the photoreactor with 50% yield. This contrasts with previous studies, where **1** was only obtained after further heating of the solution under an atmosphere of O_2[10,13,14] and there remains substantial scope for further improvement of these parameters: a key factor being the concentration of O_2, where we have limited ourselves to 2 mol%.

Table 1. Continuous `one-pot' synthesis of artemisinin from **3** using CO_2 as the reaction solvent.[a]

Entry	Co-Solvent	Catalyst	CO_2 (mL min^{-1})	**3**[b] (mL min^{-1})	Pass	Conv.[c] (%)	Yield[c] (%)
1	EtOAc	TPFPP-Amb[d]	0.53	0.05[e]	1	92	50
2	Toluene	TPFPP-Amb[d]	0.53	0.12	1	50	33
3	Toluene	TPP-Amb	0.53	0.12	1	63	25
					2	82	39
					3	93	48
					4	98	51[g]
4	Toluene[f]	TPP-Amb	0.53	0.12	1	>98	48[g]

[a] Operation at 5 °C, 18 MPa, 2 mol.% O_2. [b] Concentration of **3** is 0.5M (see ESI) [c] Reaction conversion and yield were calculated based on the integration of the relevant peaks in the ^{1}H-NMR spectrum according to internal standard (mesitylene); some material is lost via formation of **5** in the initial Schenck ene reaction, and more is lost via formation of oligomers, see Fig. 5; [d] Some leaching of TPFPP from Amberlyst-15 support was observed. [e]This experiment used a higher CO_2:**3** ratio to avoid system blockage. [f] Using a double-length reactor with double residence time in photoreactor, see ESI for details. All reactions were run at a reactor temperature of **5** °C (corresponding to a total residence time of *ca.* 10 min) to increase the formation of **4** over its regioisomers. [g] Although this strategy was not fully optimized, these conditions gave the highest yields and are those that have been used in the calculation of the E-factors in Table 3 and ESI.

Strategy 2: Reactions in aqueous mixtures of organic solvents

This strategy arose from control experiments in conventional solvents carried out in parallel to our work on liquid CO_2. When photo-oxidation of **3** was carried out as a batch reaction in conventional glassware, in carefully dried tetrahydrofuran (THF), surprisingly not a trace of **1** was obtained**,** just a complex mixture of byproducts. By contrast, with *wet, non-distilled* THF, the yields of **1** were relatively high (>60%), indicating that the reaction requires a minimum amount of water to proceed. This suggested that the reaction might perhaps be run in aqueous solvent mixtures, with corresponding benefits in the context of green chemistry. Even though reactions involving photochemically generated $^1O_2$ in the presence of H_2O have occasionally been reported,[32-34] the use of aqueous solutions in preparative photochemistry has been largely overlooked, probably because water and other protic solvents are excellent quenchers which reduce the lifetime of $^1O_2$.[35,36]

With these facts in mind, the effect of the presence of **3** on the emission lifetimes of $^1O_2$ was investigated in DCM, pure EtOH and a 1:1 (v/v) mixture of EtOH + H_2O. The results are summarized in Fig. 4. Mono-exponential decays provided good fits for all acquired traces. Plotting of reciprocal lifetimes versus the concentration of **3** yielded linear relationships for all three solvent systems, giving values for the photo-physical quenching constant (k_q) of 4.1 x 10^5, 1.6 x 10^5, and 9.6 x 10^5 $Lmol^{-1}s^{-1}$ for DCM, EtOH, and EtOH + H_2O, respectively. Surprisingly the addition of H_2O to EtOH *increases* the value of k_q — that is the rate at which $^1O_2$ reacts with **3**. This effect contrasts with the efficient quenching of $^1O_2$ in H_2O. Clearly, the addition of H_2O is less detrimental to the photo-oxidation reaction than one might anticipate by solely considering the reduced excited state lifetimes of $^1O_2$ in an aqueous system.

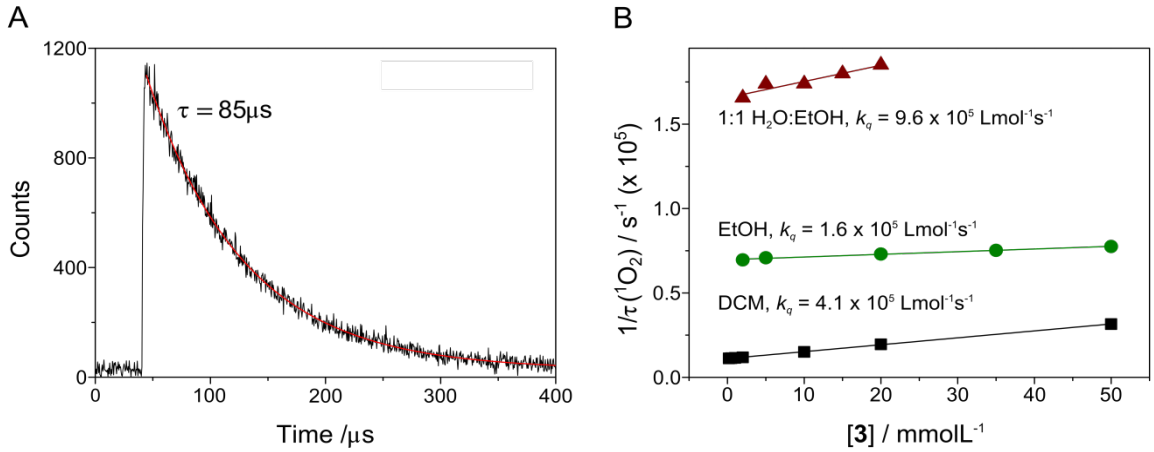

Fig. 4. $^1O_2$ emission following photo-excitation with a 355 nm pulse. (**A**) Emission trace for [**3**] = 5 $mmolL^{-1}$, in DCM, data fitted with a single exponential. (**B**) Stern-Volmer plots showing the quenching of $^1O_2$ emission by **3** in different solvent systems. The increased value of k_q indicates that $^1O_2$ can react with **3** at these concentrations, even in the presence of H_2O.

Conducting the photo-oxidation of **3** with O_2 (0.1 MPa) in mixtures of THF or EtOH with H_2O and water-soluble photosensitizers confirmed this finding; indeed, the yields of **1** were similar to those obtained in DCM and in one case higher (see Table 2, entry 2). In addition, the presence of water meant that TFA could be replaced by H_3PO_4 (entry 4), or H_2SO_4 (entries 7 - 10) which is insoluble in DCM and has been reported to promote dehydration of intermediate **6**.[14] Surprisingly, unlike many of the solvent systems previously studied,[13] the aqueous mixtures gave a high ratio of **4:5** that was essentially unchanged between – 30 °C and + 30 °C, thereby eliminating the need for energy-hungry refrigeration. The reaction also gave good yields of **1** with two different water-soluble ionic photosensitizers, $[Ru(bpy)_3]^{2+}$ or TMPyP (see Table 2).

Table 2. Solvent, photosensitizer and acid conditions screening.[a]

Entry	Solvent	Ratio	[2] mol.L^{-1}	Photosensitizer	T(°C)	Acid	Eq.	Yield[b] (%)
1	DCM		2.1 x10^{-2}	TPP	10°C	TFA	0.5	54
2	THF:H_2O	60:40	5.3 x10^{-2}	$[Ru(bpy)_3]Cl_2$	10°C	TFA	0.5	66[c]
3	THF:H_2O	60:40	5.3 x10^{-2}	$[Ru(bpy)_3]Cl_2$	30°C	TFA	0.5	59
4	THF:H_2O	60:40	5.3 x10^{-2}	$[Ru(bpy)_3]Cl_2$	0°C	H_3PO_4	0.5	52
5	THF:EtOH:H_2O	5:75:20	2.1 x10^{-2}	$[Ru(bpy)_3]Cl_2$	10°C	TFA	0.5	62
6	EtOH:H_2O	50:50	2.1 x10^{-2}	$[Ru(bpy)_3]Cl_2$	10°C	TFA	1.0	43
7	EtOH:H_2O	50:50	2.1 x10^{-2}	$[Ru(bpy)_3]Cl_2$	10°C	H_2SO_4	1.0	40
8[d]	EtOH:H_2O	80:20	1.7 x10^{-1}	$[Ru(bpy)_3]Cl_2$	0°C	H_2SO_4	0.5	50
9	EtOH:H_2O	80:20	5.3 x10^{-2}	$[Ru(bpy)_3]Cl_2$	30°C	H_2SO_4	0.5	39
10	EtOH:H_2O	60:40	2.1 x10^{-2}	TMPyP[e]	10°C	H_2SO_4	0.5	53
11	^{i}PrOH:H_2O	60:40	5.3 x10^{-2}	$[Ru(bpy)_3]Cl_2$	0°C	TFA	0.5	59

[a] Unless otherwise stated, the reactions were conducted on 250 mg scale using 1 mg of photosensitizer in a solvent volume of 20 mL. Photo-irradiation was carried out for 5 hours. [b] The yield was measured by ^{1}H NMR using mesitylene as an internal standard, added after work up. In each experiments, conversion was higher than 98%. [c] This is the highyest yield opbtained so far and was used in the calculation of E-factors in Table 3, entry 8. [d] This reaction was conducted on 6 g scale using 10 mg of photosensitizer in 150 mL solvent volume. Photo-irradiation was carried out for 8 hours. [e] 5,10,15,20-tetrakis(*N*-methylpyridinium-4-yl)porphyrin tetra(*p*-toluenesulfonate).

The overall yield of **1** was found to be higher in solutions containing THF (up to 66% yield, Table 2 entries 3-5) than in EtOH/H_2O (entries 6-10), even if only small quantities of THF were present (entry 5). THF, which is not itself a nucleophile, may well have a "protective effect" against acid-catalysed degradation, see Fig. 5.

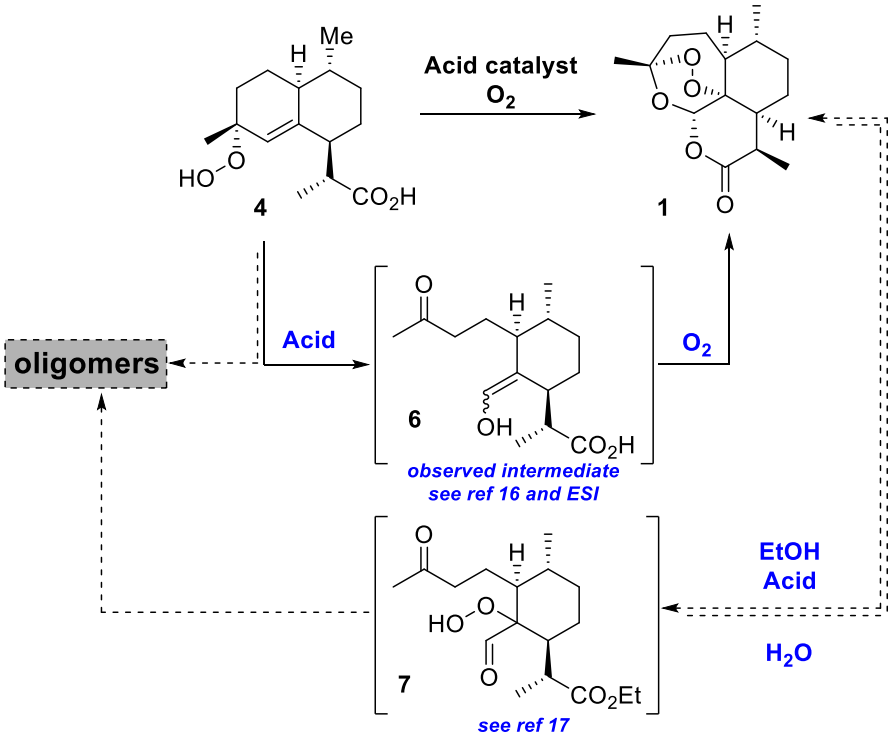

Fig. 5. Proposed acid catalyzed degradation pathways, which occur during or after the reaction and suggest why H_2O reduces the extent of degradation. Evidence for these pathways includes polar oligomeric materials (*ca.* 30-40% yield), isolated by column chromatography of the mother liquors left after crystallization of **1**; these side products were amenable to MALDI analysis (see ESI), and their presence may explain the observed yield limitations for **1**.

It seems likely that the presence of H_2O also reduces the extent of degradation by reversing the equilibrium and inhibiting radical polymerization (see Fig. 5). H_2O does, however, reduce the rate of conversion of **6** to **1** and the reaction has to be kept agitated at room temperature and

under an oxygen atmosphere for an additional period of time. We therefore attempted to deconstruct the cascade leading to **1** and found that **6** is formed with *ca.* 50% selectivity, determined by NMR using biphenyl as an internal standard (see ESI, Fig. S10). It is perhaps not surprising that the selectivity drops at that stage considering that the reaction intermediates leading to **6** are highly prone to undergoing intermolecular aldol condensation, dehydration or radical side reactions that can lead to the formation of complex oligomers, as shown by MALDI analysis (see ESI).

Given the recognized advantages of continuous processing, a flow system was implemented using EtOH/H_2O and THF/H_2O as the reaction solvents and H_2SO_4 as the acid. The reactions were carried out in the same tubular photoreactor as used with CO_2, but modified for upflow and filled with 6 mm diameter glass beads to promote mixing and reduce the optical pathlength to prevent inner filter effects, see Fig. 3D. The glass beads reduced the free volume of the reactor. Therefore, in order to maintain reasonable productivity, the conversion of **3** to **4** in THF/H_2O and EtOH/H_2O (80:20) was accelerated by using higher pressures of O_2; at a pressure of 1 MPa, the photo-conversion is largely completed at a residence time of ca. 20 min**,** (see ESI for experimental details) but as before, the final formation of **1** takes considerably longer. This is less of a problem then it might appear because it occurs in the presence of air in the product collection flask.

Perhaps, the most striking aspect of using H_2O as a reaction solvent is seen during product work up because partial evaporation of EtOH or THF from the aqueous mixtures results in the spontaneous crystallization of pure **1**, see Fig. 3B/C and ESI. At the same time, the H_2O-soluble photosensitizer and the acid remain in solution, available for continued use. Therefore, we have demonstrated the recycling of not only the aqueous solution of photosensitizer and acid catalyst but also of the evaporated EtOH for three cycles with no loss in yield of **1**. As shown in Fig. 3A, the result is a simple process where the only inputs are **3**, light, O_2 and heat; the sole output is **1**.

How do these strategies compare?

Both strategies presented above involve flow chemistry. Therefore the amount of product obtained depends on how long the reactors are run. **1** has relatively low solubility in our solvent systems [toluene + CO_2] (strategy 1) and [EtOH + H_2O] (strategy 2) and the solutions are more dilute than in published work.[10,13] However, this dilution is compensated by the efficiency of our reactors so that the space time yields in strategies 1 & 2 are 2.5 g/mL/day and 3.4 g/mL/day respectively, comparable to literature data for producing **1** by flow chemistry.[13] The reaction in aqueous solvent (strategy 2) can be operated indefinitely as reactants and catalysts are in homogeneous solution. By contrast, with liquid CO_2 (strategy 1) there is a heterogeneous catalyst and the running time will eventually be limited by bleaching of the supported porphyrin. The main differences from the literature lie in the overall processing time, temperatures and greatly reduced workup necessary to recover the product. Strategy 1 delivers **1** directly at the outflow while the aqueous chemistry in strategy 2 requires additional time for the formation of **1**. On the other hand, the aqueous strategy 2 can be used in either flow or batch processes and could easily be implemented on the existing industrial-scale plant;[10] strategy 1 would require new higher pressure equipment; however, it has already been demonstrated[21] that lab-scale tubular reactors for thermal chemistry can be successfully scaled out into parallel reactors for commercial scale production while still only using the same number of pumps and compressors as in the laboratory.

But how green are these strategies? Qualitatively, one can rate them using the Twelve Principles.[1] Although some of our experiments used TFA, both strategies can operate without

TFA, thereby avoiding toxic reagents (Principle 3). Unlike the literature[13] or industrial[10] processes, neither strategy requires a separate solvent for workup, thereby minimizing solvent usage (Principle 5). The use of CO_2 in strategy 1 does contravene Principle 6, namely that reactions should be run as close as possible to ambient temperature and pressure to minimize consumption of energy. However, both strategies run at higher temperatures than other processes and cooling is energy intensive; indeed, one paper by Seeberger's group reported that cooling their photoreactor consumed 70% of the total energy budget.[13] Apart from toluene, all of the solvents used here (i.e. THF, EtOAc, EtOH, *i*PrOH, H_2O and CO_2) are environmentally benign[37] and preferable to the halogenated solvents currently used[10] to produce **1**. In addition, EtOH, EtOAc, CO_2 and H_2O can be obtained from renewable sources (Principle 7). Both strategies avoid the derivatization required in the industrial process, as recommended by Principle 8. Finally, our strategies involve the use of organic solvents in the presence of O_2 which, without due care, could increase the chance of accidents, in contravention of Principle 12, though we mitigate the risk by adding CO_2 or H_2O.

More quantitatively, one can apply a number of metrics,[37,38] albeit only approximately as our strategies are not fully optimized and some of the required data are not available for the existing industrial process. The simplest concept is the E Factor ($kg_{waste}/kg_{product}$) based on the stoichiometry of the reaction, but ignoring water.[39] Although the underlying chemistry is the same, the theoretical E Factors for our strategies is slightly lower than for the commercial process[10] which involves the additional esterification. The actual E factors are all higher because the isolated yield is considerably less than 100%, (see Table 3, entries 1 & 2). We now assess the data on the strategies in terms of two factors, E_1 and E_2. E_1, is defined as the weight of all waste per unit weight of **1;** that is including all reagents, catalysts, and solvents used for the reaction *and* the work up (but excluding water, and O_2). E_2 is the same as E_1 but excluding all of the solvents. In addition for strategy 1, we calculate E_1 with and without including CO_2. All values are summarized in Table 3.

Bearing in mind that all values are necessarily approximate, Table 3 (entries 3-5) indicates that strategy 1 with an assumed 90% recycle of CO_2 has an *unoptimized* value of E_1 similar to that of the industrial process.[10] It has a somewhat higher E_2 value largely because we have assumed a single use of the Amberlyst. By contrast, strategy 2 (entries 6-8) has higher values of E_1 than either the industrial process or strategy 1, largely because of the lower solubility of **1** in aqueous mixtures; E_1 drops, substantially on recycle (see entry 8, and Fig 3A). Of course, solvent could be recycled in any of the processes but the beauty of strategy 2 is that the solvent, acid and photocatalyst can all be recycled directly *without* purification. Obviously, such recycling will be limited by the build-up of side products and could not be carried out indefinitely but the impact of recycling on E_1 is large. E_2 factors for Strategy 2 are substantially lower than for the other processes and the solvent, EtOH, is one of the highest rated in terms of its Renewability Index.[37] Sheldon[40] has suggested that one should introduce and Environmental Quotient, Q to reflect the relative toxicity of the various wastes. In this context, it is particularly important that both strategies eliminate the need for DCM as a solvent and that strategy 2 provides an opportunity to eliminate TFA (entries 6 & 7).

Entry 8 shows that one could reduce the E factors dramatically by increasing the yield of **1** and our strategies do have features which suggest that some increase may be possible following further optimization, namely the reduction in acid-induced decomposition of **1 (**either by use of a solid acid resin or by the presence of H_2O), and secondly the observation that even small amounts of THF have a positive effect on yield of **1** Table 2.

Table 3: Comparison of E factors for Strategies 1 & 2 and the commercial process for making **1** (details of the calculations are presented in the ESI)

Entry	Process	Photocatalyst/ Acid Catalyst	Solvent(s)	Yield	E_1 (no water)	E_2 (no solvent)
1	Theoretical[a]	–	–	100%	0 (0.45)[b]	0 (0.45)[b]
2		–	–	50%	0.84	0.84
3	Sanofi[c]	TFA, TPP	DCM, Heptane[d]	55%	36	4.8
4	Strategy 1 (Table 1 entry 3)	Amberlyst/TPP[e]	Toluene/liq CO_2 (4 passes)	39%	23 [f] (97)[g] (31)[h]	8
5	Strategy 1 (Table 1, entry 4)	Amberlyst/TPP[e]	Toluene/liq CO_2 (long reactor, single pass)	39%	30[f] (104)[g] (37)[h]	15
6	Strategy 2 (Table S4, entry 15)	H_2SO_4, $Ru(bpy)_3^{2+}$	EtOH/H_2O[i]	38%	210	1.8
7	Strategy 2 (Table S4, entry 15 & Scheme S6)	H_2SO_4, $Ru(bpy)_3^{2+}$	EtOH/H_2O[i] (3 cycles)	37%	101	1.5
8	Strategy 2 (Table 2, entry 2)	TFA, $Ru(bpy)_3^{2+}$	THF/H_2O[j]	(50%)[k]	73	1.3

[a] Based on the stoichiometric equation for **2** → **1**; [b] Numbers in parentheses for the Sanofi process[10] including the waste from the esterification step; [c] see ref 10, for this and other processes, the amount of O_2 has been ignored as insufficient data are available; [d] Requires additional solvents, EtOH and H_2O for purification; [e] Assuming that the Amberlyst TPP is damaged and cannot be used for further reactions; [f] Ignoring the CO_2; [g] including mass of CO_2; [h] Assuming a recycle of CO_2 with a 10% loss in each cycle as found in industrial hydrogenation in $scCO_2$, see Ref 21; [i] EtOH:H_2O 80:20; [j] THF:H_2O 60:40; [k] In this experiment, **1** was obtained in solution with 66% yield but not isolated – therefore 50% isolated yield has been assumed.

Conclusions

The conversion of **3** to **1** is intriguingly complex. We have shown that application of the principles of green chemistry has opened up a wider range of options for carrying out this transformation. Liquid CO_2 offers interesting possibilities, especially in process safety because of the inertness of CO_2 towards oxidation and in the possibility of implementing a continuous process. However, the more immediate impact is likely to come from conventional solvents. The use of aqueous mixtures offers the opportunity for solvent manipulations, particularly in the work up of the product, that are not possible with the solvents currently used in this process. In addition, the reaction can be carried out at near ambient temperatures in the presence of water, thereby eliminating the need for energy demanding refrigeration. Some of the approaches described here hold promise for rapid implementation on a larger scale, thereby taking us a step closer to more affordable artemisinin with benefits not only to malaria sufferers across the world but also to the producers of *Artemisia annua* by giving added value to their crop which, apart from **1**, can additionally yield **2**, the starting material for the semi-synthetic route.

As pointed out over a century ago,[41] photochemistry has great potential for chemical manufacture. However, it is only quite recently that the need for cleaner processes to make complex molecules has reawakened interest in process photochemistry, and the strategies introduced here are applicable to chemistry beyond transforming **2** into **1**. Liquid CO_2 probably has the lowest cost of any solvent obtainable in high purity which is important in processing pharmaceutical chemicals. Ion exchange resins such as Amberlyst could be used to immobilize a wider range of homogeneous catalysts, in addition to photocatalysts, to generate dual- or multi-functional immobilized catalysts. Our use of aqueous mixtures of common solvents is a timely reminder that mixing solvents can generate a tunability of properties reminiscent of more expensive 'designer' solvents.[42] Finally, we have demonstrated that applying the principles of

green chemistry to even well-studied reactions can lead to new and unexpected approaches which have potential processing benefits beyond being greener.

1 Anastas, P. T. & Warner, J. C. *Green Chemistry: Theory and Practice*. (Oxford University Press, 1998).
2 Tang, S. Y., Bourne, R. A., Smith, R. L. & Poliakoff, M. The 24 Principles of Green Engineering and Green Chemistry: "IMPROVEMENTS PRODUCTIVELY". *Green Chem.* **10**, 268-269 (2008).
3 Dunn, P. J., Galvin, S. & Hettenbach, K. The development of an environmentally benign synthesis of sildenafil citrate (Viagra) and its assessment by Green Chemistry metrics. *Green Chem.* **6**, 43-48 (2004).
4 Klayman, D. L. Qinghaosu (artemisinin): an antimalarial drug from China. *Science* **228**, 1049-1055 (1985).
5 Paddon, C. J. & Keasling, J. D. Semi-synthetic artemisinin: a model for the use of synthetic biology in pharmaceutical development. *Nat. Rev. Microbiol.* **12**, 355-367 (2014).
6 Westfall, P. J. *et al.* Production of amorphadiene in yeast, and its conversion to dihydroartemisinic acid, precursor to the antimalarial agent artemisinin. *Proc. Natl. Acad. Sci.* **109**, E111-E118 (2012).
7 Bauer, A. & Bronstrup, M. Industrial natural product chemistry for drug discovery and development. *Nat. Prod. Rep.* **31**, 35-60 (2014).
8 Paddon, C. J. *et al.* High-level semi-synthetic production of the potent antimalarial artemisinin. *Nature* **496**, 528-532 (2013).
9 Feth, M. P., Rossen, K. & Burgard, A. Pilot plant PAT approach for the diastereoselective diimide reduction of artemisinic acid. *Org. Process Res. Dev.* **17**, 282-293 (2013).
10 Turconi, J. *et al.* Semisynthetic artemisinin, the chemical path to industrial production. *Org. Process Res. Dev.* **18**, 417-422 (2014).
11 Roth, R. J. & Acton, N. A Simple conversion of artemisinic acid into artemisinin. *J. Nat. Prod.* **52**, 1183-1185 (1989).
12 Acton, N. & Roth, R. J. On the conversion of dihydroartemisinic acid into artemisinin. *J. Org. Chem.* **57**, 3610-3614 (1992).
13 Kopetzki, D., Lévesque, F. & Seeberger, P. H. A Continuous-Flow Process for the Synthesis of Artemisinin. *Chem. Eur. J.* **19**, 5450-5456 (2013).
14 Lévesque, F. & Seeberger, P. H. Continuous-Flow Synthesis of the Anti-Malaria Drug Artemisinin. *Angew. Chem. Int. Ed.* **51**, 1706-1709 (2012).
15 Sy, L.-K. & Brown, G. D. The mechanism of the spontaneous autoxidation of dihydroartemisinic acid. *Tetrahedron* **58**, 897-908 (2002).
16 Sy, L.-K. & Brown, G. D. The role of the 12-carboxylic acid group in the spontaneous autoxidation of dihydroartemisinic acid. *Tetrahedron* **58**, 909-923 (2002).
17 Singh, C., Chaudhary, S., Kanchan, R. & Puri, S. K. Conversion of Antimalarial Drug Artemisinin to a New Series of Tricyclic 1,2,4-Trioxanes. *Org. Lett.* **9**, 4327-4329 (2007).
18 Worrall, D. R., Abdel-Shafi, A. A. & Wilkinson, F. Factors affecting the rate of decay of the first excited singlet state of molecular oxygen in supercritical fluid carbon dioxide. *J. Phys. Chem. A* **105**, 1270-1276 (2001).
19 Leitner, W., Jessop, P. G. & Editors. *Handbook Of Green Chemistry, Volume 4: Supercritical Solvents*. (Wiley-VCH Verlag GmbH & Co. KGaA, 2010).
20 Han, X. & Poliakoff, M. Continuous reactions in supercritical carbon dioxide: problems, solutions and possible ways forward. *Chem. Soc. Rev.* **41**, 1428-1436 (2012).
21 Licence, P., Ke, J., Sokolova, M., Ross, S. K. & Poliakoff, M. Chemical reactions in supercritical carbon dioxide: from laboratory to commercial plant. *Green Chem.* **5**, 99-104 (2003).
22 Bourne, R. A., Han, X., Poliakoff, M. & George, M. W. Cleaner continuous photo-oxidation using singlet oxygen in supercritical carbon dioxide. *Angew. Chem. Int. Ed.* **48**, 5322-5325 (2009).
23 Han, X., Bourne, R. A., Poliakoff, M. & George, M. W. Immobilised photosensitisers for continuous flow reactions of singlet oxygen in supercritical carbon dioxide. *Chem. Sci.* **2**, 1059-1067 (2011).
24 Han, X., Bourne, R. A., Poliakoff, M. & George, M. W. Strategies for cleaner oxidations using photochemically generated singlet oxygen in supercritical carbon dioxide. *Green Chem.* **11**, 1787-1792 (2009).

25 Hall, J. F. B., Han, X., Poliakoff, M., Bourne, R. A. & George, M. W. Maximising the efficiency of continuous photo-oxidation with singlet oxygen in supercritical CO_2 by use of fluorous biphasic catalysis. *Chem. Commun.* **48**, 3073-3075 (2012).
26 Hall, J. F. B. *et al.* Synthesis of antimalarial trioxanes via continuous photo-oxidation with $^1O_2$ in supercritical CO_2. *Green Chem.* **15**, 177-180 (2013).
27 Griesbeck, A. G., El-Idreesy, T. T. & Bartoschek, A. Photooxygenation in polystyrene beads with covalently and non-covalently bound tetraarylporphyrin sensitizers. *Adv. Synth. Cat.* **346**, 245-251 (2004).
28 Johnson Inbaraj, J., Vinodu, M. V., Gandhidasan, R., Murugesan, R. & Padmanabhan, M. Photosensitizing properties of ionic porphyrins immobilized on functionalized solid polystyrene support. *J. App. Pol. Sci.* **89**, 3925-3930 (2003).
29 Ribeiro, S. M., Serra, A. C. & Rocha Gonsalves, A. M. d. A. Immobilised porphyrins in monoterpene photooxidations. *J. Catalysis* **256**, 331-337 (2008).
30 Ribeiro, S., Serra, A. C. & A. Rocha Gonsalves, A. M. d. Efficient solar photooxygenation with supported porphyrins as catalysts. *ChemCatChem* **5**, 134-137 (2013).
31 Neuberger, A. & Scott, J. J. The basicities of the nitrogen atoms in the porphyrin nucleus; their dependence on some substituents of the tetrapyrrolic ring. *Proc. Roy. Soc. Lond. Math. Phys. Sci.* **213**, 307-326 (1952).
32 Frederiksen, P. K. *et al.* Two-photon photosensitized production of singlet oxygen in water. *J. Am. Chem. Soc.* **127**, 255-269 (2004).
33 Jensen, R. L., Arnbjerg, J. & Ogilby, P. R. Reaction of singlet oxygen with tryptophan in proteins: a pronounced effect of the local environment on the reaction rate. *J. Am. Chem. Soc.* **134**, 9820-9826 (2012).
34 Yavorskyy, A. *et al.* Photooxygenations in a bubble column reactor. *Green Chem.* **14**, 888-892 (2012).
35 Zepp, R. G., Wolfe, N. L., Baughman, G. L. & Hollis, R. C. Singlet oxygen in natural waters. *Nature* **267**, 421-423 (1977).
36 Lindig, B. A., Rodgers, M. A. J. & Schaap, A. P. Determination of the lifetime of singlet oxygen in water-d_2 using 9,10-anthracenedipropionic acid, a water-soluble probe. *J. Am. Chem. Soc.* **102**, 5590-5593 (1980).
37 Jimenez-Gonzalez, C., Constable & D. J. C. Ponder, C. S., Evaluating the ‘‘Greenness’’ of chemical processes and products in the pharmaceutical industry—a green metrics primer, *Chem. Soc. Rev.,* **41**, 1485–1498, (2012).
38 Calvo-Flores, F. G., Sustainable Chemistry Metrics, *ChemSusChem* **2**, 905 – 919 (2009)
39 Sheldon, R. A. The E factor: fifteen years on, *Green Chem.* **9***,* 1273-1283, (2007).
40 Sheldon, R. A. Consider the Environmental Quotient, *CHEMTECH,* **24**, 38-47 (1994).
41 Ciamician, G. The photochemistry of the future. *Science* **36**, 385-394 (1912).
42 Freemantle, M. *Ionic Liquids as Designer Solvents*. Roy. Soc. Chem., Cambridge (2010) ISBN 978-1-84755-161-0

Acknowledgments:

We thank Sanofi, the University of Nottingham and the Bill and Melinda Gates Foundation Grant No. 1070294, and EPSRC Grant No. EP/L021889/1 (Continuous Chemical Manufacture with Light) for supporting this research. JFBB thanks the EPSRC for a studentship and MWG thanks the Royal Society for a Wolfson Merit Award. We thank L. Hitchen for her contribution to batch studies in $scCO_2$, M. Guyler, P Fields, R. Wilson and D Litchfield for technical support. G. Coxhill for the MALDI analysis and Dr W. Lewis for obtaining crystal structure of **1**, shown in Fig. 4. We thank D. B. Amabilino and P. Licence for their helpful comments. Note that the production of semi-synthetic **1** at Sanofi is a not-for-profit venture, its development being supported in part by the Bill and Melinda Gates Foundation.

Additional information

Supplementary Materials
Materials and Methods
Figs. S1 to S10
Tables S1 to S7
Schemes S1 to S12

Applying Green Chemistry to the Photochemical Route to Artemisinin

Zacharias Amara,[a] Jessica F. B. Bellamy,[a] Raphael Horvath,[a] Samuel J. Miller,[a] Andrew Beeby,[b] Andreas Burgard,[c] Kai Rossen,*[c] Martyn Poliakoff*[a] and Michael W. George*[a]

[a] School of Chemistry, University of Nottingham, University Park, Nottingham, NG7 2RD, UK. [b] Department of Chemistry, University of Durham, South Rd, Durham DH1 3LE, UK. [c] Sanofi-Aventis Deutschland GMBH, C&BD Frankfurt Chemistry, Process research, Industriepark Hoechst. D-65926 Frankfurt am Main, Germany.

SUPPLEMENTARY MATERIALS

Table of Contents

5. Continuous flow experiments in aqueous mixtures
   5.1. High Pressure Continuous Flow Equipment
   5.2. Adjustments of the reaction parameters for photo-oxygenation
6. Green Metrics Calculations

1. Characterization and spectral data for an isolated sample of 1 and comparison with an authentic sample of 1 from the commercial process.
2. Crystal data
3. Analysis of impurities from reaction mixture table S4, entry 16

1. Materials and methods

1.1. General

Reagents and solvents were used as received, without further purification, unless otherwise noted. Oxygen (>99.5%) and carbon dioxide (food grade) were obtained from BOC and used as received. Photosensitizers, **PS** (Figure S1) and trifluoroacetic acid were purchased from Sigma Aldrich. Amberlyst® 15 (dry) was purchased from Acros Organics, sulfuric acid (>95%) was purchased from Fisher Chemicals and *ortho*-phosphoric acid (85%) was purchased from Fluka analytical. Dihydroartemisinic acid (**3**) was supplied by Sanofi-Aventis. Solvents were purchased from VWR Prolabo and used without further purification. Photochemical experiments were carried out using a bank of Citizen Electronics Co. Ltd 1000 lumen white light LEDs (arranged in 3 sets of 5 diode arrays).

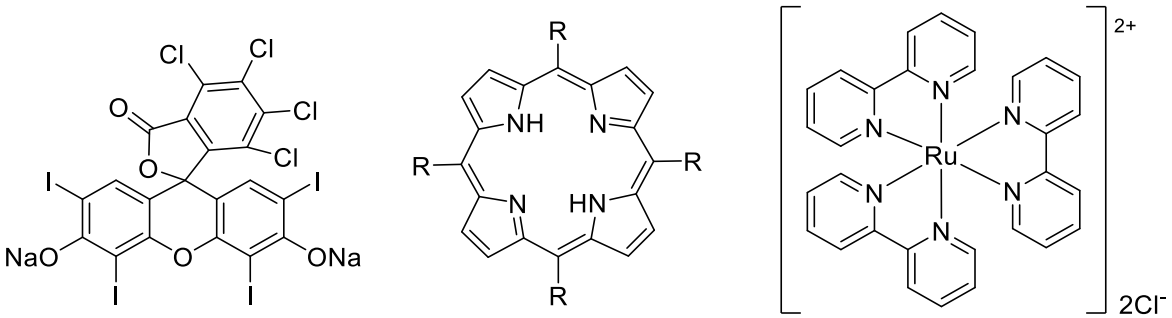

Rose Bengal
Sodium Salt (RB)

TPFFPP, R=C_6F_5
TPP, R=C_6H_5
TMPyP, R=*N*-MePy$^+$pTsO$^-$

$[Ru(bpy)_3]Cl_{2.6}H_2O$

Figure S1: Structures of the photosensitizers (PS) tested in this study.

1.2. Characterization

^{1}H spectra were recorded on a Bruker DPX300, or Bruker AV(III)400 spectrometer at 300 MHz and 400 MHz respectively. ^{13}C spectra were recorded on a Bruker AV(III)500 spectrometer at 125 MHz respectively. The analysis was carried out using ACD/SpecManager software version 12 and spectra were referenced to $CDCl_3$ (7.27 ppm for ^{1}H-NMR, 77.00 ppm for ^{13}C-NMR), C_6D_6 (7.16 ppm for ^{1}H-NMR) or Acetone-d_6 (2.05 ppm for ^{1}H-NMR). The pH measurements were carried out using a Metrohm 785 DMP Trinito pH meter. Mass spectrometry analyses were performed using Bruker microTOF equipped with an Electron Spray Ionization method and with a Bruker Ultraflex III equipped with a Matrix Laser Desorption Ionization source.

1.3. Spectroscopic measurements

Diffuse reflectance measurements of the immobilized porphyrins were acquired using an Ocean Optics USB2000+ UV-vis spectrometer, equipped with an Ocean Optics UV-Vis-NIR light source (DT-MINI-2-GS) fitted with a fiber optic (part number P200-2-VIS-NIR). Spectra were collected using Ocean Optics SpectraSuite (version 6.1) against a silicon zero diffraction plate. The ethyl acetate solution spectra of the protonated porphyrins were recorded using a Perkin Elmer Lambda 25 UV-visible spectrometer.

Singlet oxygen emission measurements were carried out on air-equilibrated solutions of CH_2Cl_2, EtOH, and 1:1 mixtures of EtOH:H_2O. Oxygenation of solutions with photosensitizer was found to increase the emission intensity while negligibly affecting the excited state lifetimes. Additional oxygenation of the samples containing **3** was not performed in order to maintain better control over the concentration of each solution. The sample was held in a 10 mm quartz cuvette with the concentration of photosensitizer adjusted to give an absorbance at the excitation wavelength of 0.3. Emission traces were recorded at 1270 nm after

photoexcitation at 355 nm (GCR150-10, 10 Hz, ~1 mJ per pulse). Emission was collected at a 90° angle, the emission wavelength selected with a monochromator (TRIAX-320) and passed onto a NIR-PMT (Hamamatsu H10330A-45) controlled by LabVIEW. The resulting emission traces were fitted as exponential decays. Approximately 10000 shots were acquired for each trace. The bimolecular quenching constant of **3** (k_q), assumed to be equivalent to the rate constant of photo-oxidation, was evaluated by plotting the reciprocal of the quenched emission lifetime ($\frac{1}{\tau}$) against the concentration of **3** ([Q]) according to the Stern-Volmer relationship:

$$\frac{1}{\tau} = k_q[\mathrm{Q}] + \frac{1}{\tau_0}$$

where τ_0 is the unquenched emission lifetime.

2. Synthesis of artemisinin in CO_2

2.1. High pressure continuous flow equipment

The continuous flow photo-oxidation reactor system, for reactions with $^1O_2$, consists of a custom-built sapphire tube reactor (shown in Figure S3), stainless steel tubing and a series of liquid pumps and valves, as shown in Figure S2. HPLC pumps supply CO_2, the organic feed and any co-solvent required to improve solubility. O_2 is dosed into the system *via* a modified Rheodyne switching valve and is supplied at cylinder pressure. CO_2 and O_2 are mixed using a static mixer, which is heated to 50 ^oC prior to mixing with the organic stream(s). The fluid then flows through the sapphire tube reactor where it is subjected to visible light irradiation using an array of LEDs. The pressure of the system is controlled at its outlet using a BPR and the product is collected at this point.

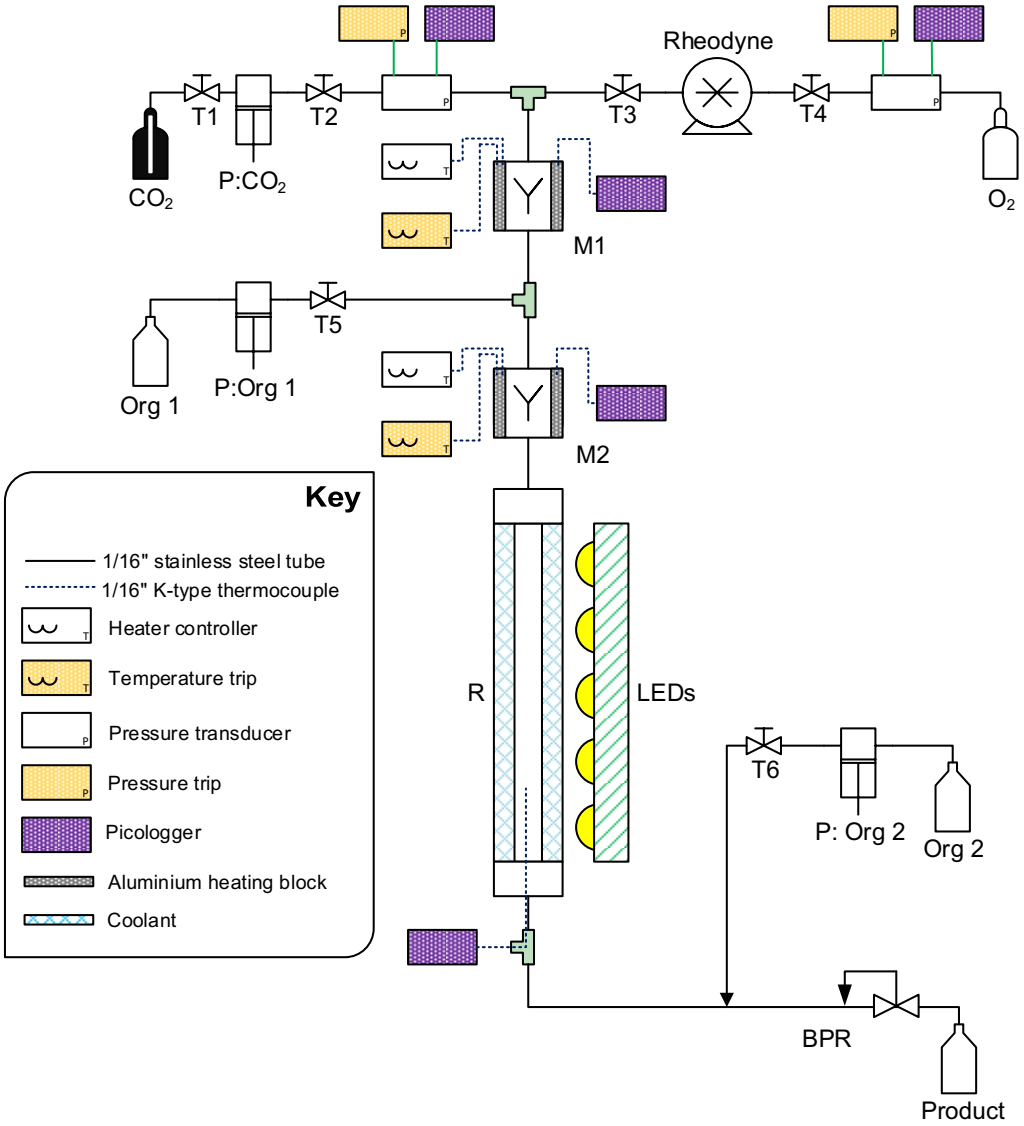

Figure S2: Schematic of the CO_2 reactor used. CO_2 is delivered by **P:CO₂** (a Jasco™ PU-1580-CO_2 HPLC pump), O_2 is added using a modified **Rheodyne** dosage unit. **Org 1**: **3** is dissolved in the required co-solvent (+ PS and acid as required) which is pumped by **P:Org 1** (a Jasco™ PU-980 HPLC pump); **Org 2**: co-solvent added in systems which are subject to blockage pumped *via* **P:Org 2** (a Jasco™ PU-980 HPLC pump); **M1 & M2**: static mixers (stainless steel tubing ¼" o.d., 75 mm in length packed with sand and heated *via* temperature controlled aluminium blocks); **R**: sapphire tube reactor which is temperature controlled *via* a circulating water/ethylene glycol bath (Grant LTD6/20); **LEDs**: light source (3 × 5 × Citizen Electronics Co. Ltd CL-L233-C13 N mounted on water cooled stainless steel blocks); **BPR**: back pressure regulator (model Jasco™ BP 1580-81); **T*N***: (where N is a number) manual valve. Where a heterogeneous acid was required, a stainless steel tube (1/4" o.d., 75 mm length) packed with acid was inserted following **R** and prior to **P:Org 2** and the temperature was controlled *via* aluminium heating blocks. **Picologger** monitors system and oxygen pressures, internal reactor, mixers and cooling bath temperatures.

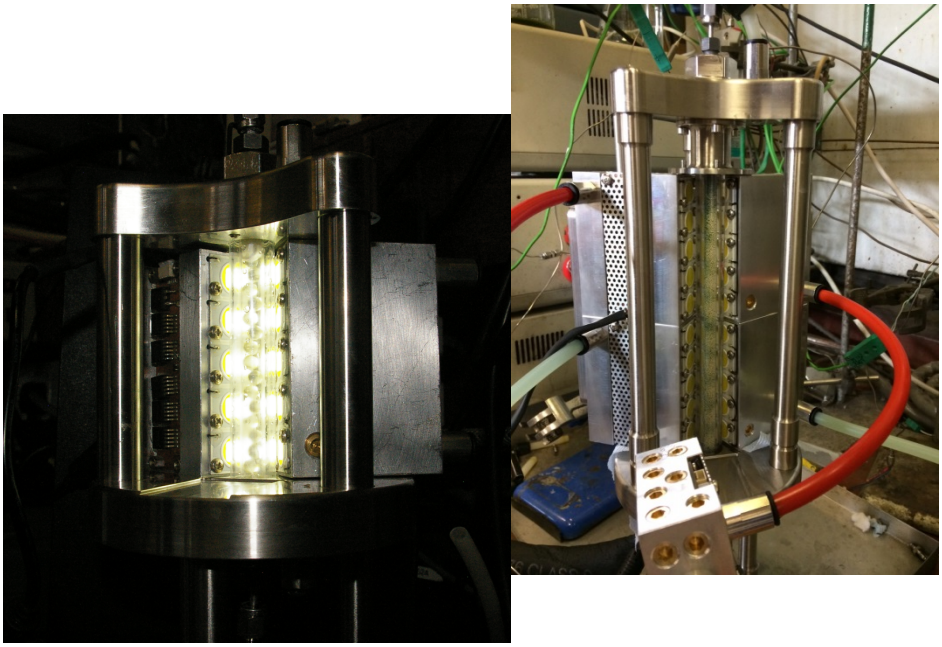

Figure S3: Picture of the sapphire tube reactors used for high pressure photo-oxidations. A sapphire tube (Saint-Gobain Crystals, 10 mm o.d., **120 or 240** mm long, 1 mm wall thickness) is held in place and sealed with two EPDM O-rings. A Lexan™ polycarbonate tube surrounds the sapphire tube and coolant is flowed in the space between the two tubes from bottom to top. The high pressure fluid enters the sapphire tube through the top of the reactor and leaves through the bottom. The sapphire tube is filled with glass beads in this image for clarity.

2.2. Photo-oxidation of dihydroartemisinic acid in CO_2

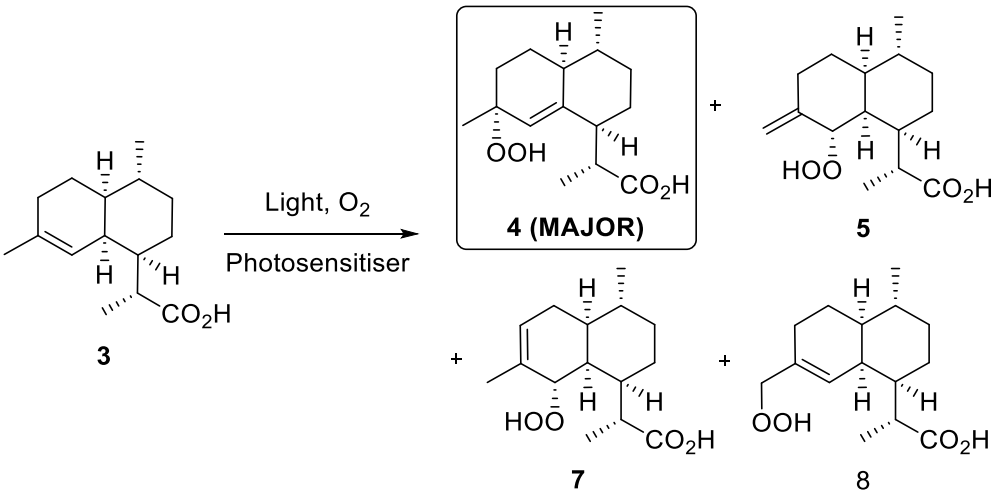

Scheme S1: Photo-oxidation of **3**.

10 g of **3** (42.4 mmol) was dissolved in ethyl acetate (75 mL) together with the desired amount of TPFPP. This solution was then pumped and mixed into a flowing stream of CO_2/O_2 *prior* to irradiation in the sapphire tube photoreactor. The effect of flow rate, oxygen and TPFPP concentrations on the conversion of **3** was investigated. For all experiments, the system pressure was maintained at 180 bar and the concentration of **3** in the high pressure system was 0.10 M. Initially, the photoreactor temperature was maintained at 40 ^{o}C, to ensure supercritical conditions, but it was found that lowering the temperature to 5 ^{o}C was beneficial in terms of selectivity towards the desired product **4**. The crude product, collected directly following depressurization, was dried under vacuum and analyzed by ^{1}H-NMR, with $CDCl_3$ as the solvent.

Table S1: Continuous flow photo-oxidation of **3** to **4**

Entry	CO_2 (mL.min^{-1})	Org. (mL.min^{-1})	O_2:3 (mol:mol)	[TPFPP] mol%	T (°C)	Conv. of 3 (%)	Selectivity of 4 (%)[a]
1	0.53	0.12	2:1	0.10	40	96	63
2	0.80	0.20	2:1	0.10	40	94	64
3	1.05	0.25	2:1	0.10	40	92	68
4	1.60	0.40	2:1	0.10	40	85	65
5	2.10	0.50	2:1	0.10	40	81	64
6	1.05	0.25	1:1	0.05	40	83	59
7	1.05	0.25	2:1	0.05	40	82	63
8	1.05	0.25	3:1	0.05	40	83	59
9	1.05	0.25	4:1	0.05	40	87	62
10	1.05	0.25	2:1	0.03	40	63	54
11	1.05	0.25	2:1	0.05	40	80	68
12	1.05	0.25	2:1	0.10	40	90	75

13	1.05	0.25	2:1	0.17	40	94	68
14	1.05	0.25	2:1	0.24	40	64	65
15	0.53	0.12	2:1	0.10	5	91	75

[a] In each experiment, the selectivity was measured by ^{1}H NMR in $CDCl_3$

2.3. Synthesis of artemisinin from dihydroartemisinic acid in CO_2

For the synthesis of artemisinin (**1**) from **3** using the high pressure CO_2 system, three different strategies were explored: Methods A, B and C as described below. For all experiments, the photo-oxidation was carried out in the sapphire tube reactor (figure S3), the system pressure was maintained at 180 bar and the temperature was 5 °C and the O_2:**3** molar ratio was 2:1. Samples were analyzed by ^1H NMR in $CDCl_3$ after removal of the volatiles under reduced pressure. The results are summarized in Table S2 below.

2.3.1. Method A: One pot homogeneous synthesis of artemisinin in CO_2

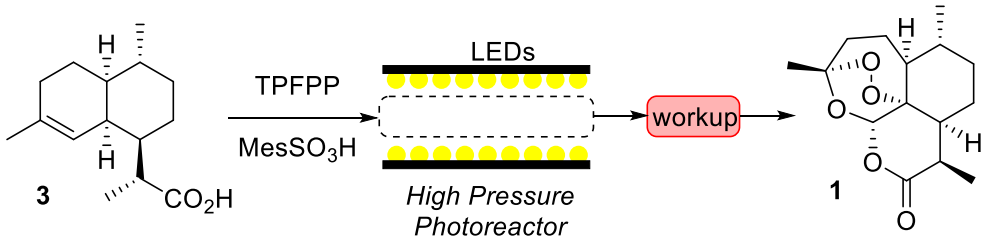

Scheme S2: Process of the one pot homogeneous synthesis in CO_2.

The homogeneous one pot synthesis of **1** from **3** (Scheme S2) was conducted as described for the photo-oxidation procedure but 2-mesitylene sulfonic acid ($MesSO_3H$, 4.2 mmol, 1 g, 0.5 eq) was added to the starting solution containing 2 g of **3** (8.5 mmol) and TPFPP (8 mg, 1 mol%) in ethyl acetate (50 mL, 0.17 M). Samples were analyzed without acid neutralization after removal of the volatiles under vacuum and $MesSO_3H$ was used as an internal standard.

Note: no artemisinin crystals could be obtained without acid neutralization.

2.3.2. Method B: Sequential synthesis of artemisinin in CO_2

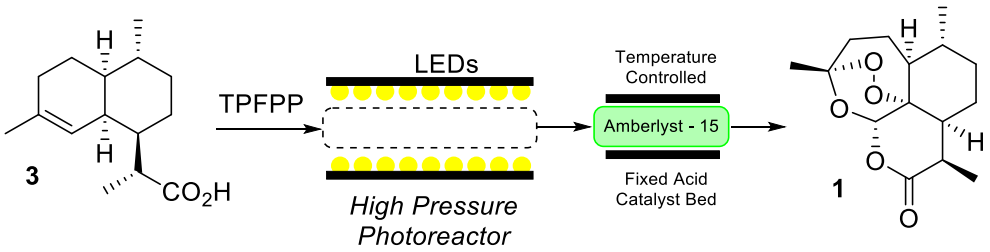

Scheme S3: Process of the sequential synthesis in CO_2.

The sequential homogeneous/heterogeneous synthesis of **1** from **3** (Scheme S3) was conducted as described for the photo-oxidation procedure but a second reactor (stainless steel tubing, ¼" o.d., 75 mm length), packed with amberlyst-15 (dry, beads, *ca.* 1 g), was added downstream. The temperature of this reactor was maintained *via* heating blocks at 25 ^{O}C. A starting solution of **3** (4 g, 17 mmol) and TPFPP (16 mg, 1 mol%) in ethyl acetate (30 mL, 0.5M) was used.

2.3.3. Method C: One pot heterogeneous synthesis of artemisinin in CO_2

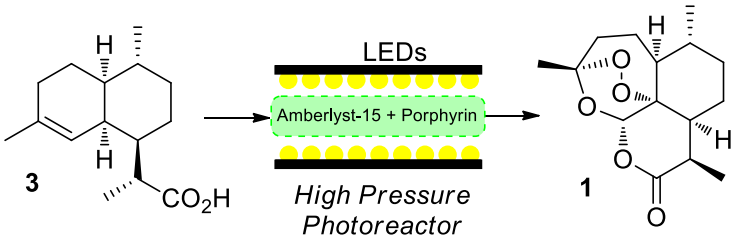

Scheme S4: Process of the one pot heterogeneous synthesis in CO_2

1 g of **3** (4.2 mmol) was dissolved in either ethyl acetate (8 mL) or toluene (8 mL) and the solution was pumped at 0.125 mL.min^{-1} into a CO_2/O_2 stream (0.525 mL.min^{-1}, 2.3% O_2) at 180 bar pressure. The molar ratio of O_2:**3** was maintained at 5:1. The reaction stream was passed through the photoreactor containing a porphyrin immobilized on Amberlyst-15 (see below). In order to realize full conversion of **3**, the product solution following depressurization was collected and re-passed through the reactor multiple times. The results are presented in Table S2.

- **Preparation of porphyrins immobilized on Amberlyst-15**

In an opened round bottom flask equipped with a magnetic stirrer, 100 mg of TPP or TPFPP (0.16 or 0.10 mmol) was dissolved in EtOAc (50 mL) and added with Amberlyst-15 beads (3 g). The heterogeneous mixture was slowly agitated at room temperature for 24 h. The resulting heterogeneous mixture was then filtered and washed with EtOAc (3 x 10 mL) to yield green

beads that were dried under vacuum. Loading of TPFPP was calculated to be 18 mg.g^{-1}. Loading of TPP was calculated to be 17 mg.g^{-1}.

- **Characterization of catalyst systems**

The porphyrin-Amberlyst-15 systems were characterized by UV-visible absorption spectroscopy and spectra were compared to the protonated 2-mesitylenesulfonate salts (see Figure S4). The diffuse reflectance spectra of TPP and TPFPP bound to Amberlyst show absorption peaks at *ca.* 660 nm and 575/630 nm respectively, which is indicative of the protonated porphyrin species, as indicated by the solution spectra. Similarly, major bands at 512 nm and 504 nm in the solution spectra of neutral TPP and TPFPP respectively are absent in the corresponding diffuse reflectance spectra.

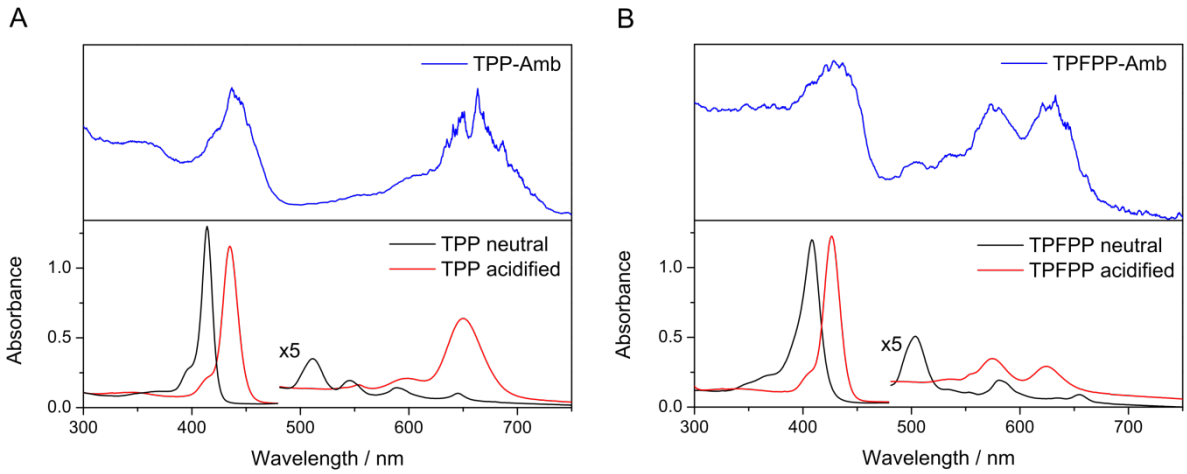

Figure S4: Anchoring of photosensitizers investigated by UV-visible spectroscopy. **Blue:** The diffuse reflectance spectra obtained for TPP (A) and TPFPP (B) immobilized on Amberlyst-15, with applied Kubelka Munk correction (offset). **Red:** The solution spectrum of protonated TPP (A) and TPFPP (B) at a concentration of 1.5 x 10^{-4} molL^{-1} recorded in ethyl acetate with a path length of 400 µm. **Black:** The solution spectrum of neutral TPP (A) and TPFPP (B) at a concentration of 1.5 x 10^{-4} molL^{-1} recorded in ethyl acetate with a path length of 400 µm.

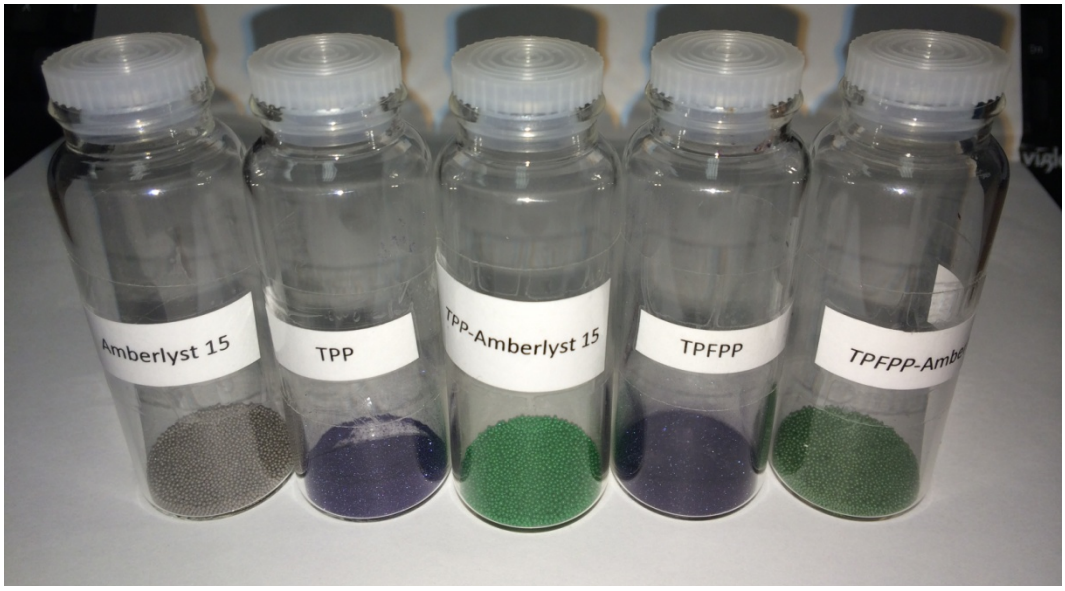

Figure S5: Picture of Amberlyst-15 and supported porphyrin systems, showing the differences in color.

Table S2: Results for the one pot CO_2 synthesis of artemisinin (the organic feed containing **3** is at a concentration of 0.5M, the concentrations in this table are calculated by taking CO_2 into account).

Entry	Co-Solvent	Method[a]	PS	CO_2 ($mL.min^{-1}$)	Org. ($mL.min^{-1}$)	[3] ($mol.L^{-3}$)	Pass	Conv (%)	Yield[b] (%)	Reactor Blockage
1	EtOAc	**A**	TPFPP	1.05	0.25	0.1	-	-	-	Yes
2	EtOAc	**A**	TPFPP	1.05	0.25	0.03	1	67	47[c]	No
3	EtOAc	**A**	TPFPP	0.53	0.12	0.03	1	80	56[c]	No
4	EtOAc	**B**	TPFPP	1.05	0.25	0.1	1	77	50	No
5	EtOAc	**C**	TPFPP	0.53	0.12	0.1	1	75	47	Yes
6[d]	EtOAc	**C**	TPFPP	0.53	0.05	0.05	1	92	50	No
7	Toluene	**C**	TPFPP	0.53	0.12	0.1	1	50	33	No
8	Toluene	**C**	TPP	0.53	0.12	0.1	1	63	25	No
9	Toluene	**C**	TPP	0.53	0.12	0.1	2	82	39	No

10	Toluene	**C**	TPP	0.53	0.12	0.1	3	93	48	No
11	Toluene	**C**	TPP	0.53	0.12	0.1	4	98	51	No
12[e]	**Toluene**	**C**	**TPP**	**0.53**	**0.12**	**0.1**	**1**	**>98%**	**49**	**No**

[a] In each experiment, the pressure was 180 bar with a concentration of O_2 of 2 mol.%. The photoreactor temperature was 5 °C during operation. In the case of Methods A and B, TPFPP was used as the homogeneous photosensitizer at a concentration of 0.1 mol%. [b] In each experiment, yields were measured by ^{1}H NMR in $CDCl_3$. [c] 2-mesitylenesulfonic acid was used as an internal standard . [d] Mesitylene was added following depressurization to the dried samples and used as an internal standard. [d] This experiment used a higher CO_2:**3** ratio to prevent system blockage. **3** dissolved in EtOAc (0.5 M) was pumped at 0.05 mL.min^{-1} into the CO_2/O_2 stream (0.53 mL.min^{-1}). [e] This experiment was carried out using a double length reactor described in picture S3.

UV-visible absorption spectra of the product solutions collected following reaction using the relevant porphyrin-Amberlyst-15 system were recorded (Figure S7). In both cases, 16.8 g of the crude product was dissolved in 10 ml of ethyl acetate. From these spectra, it can clearly be seen that TPFPP leeches from the Amberlyst-15 support but TPP remains immobilized throughout the experiment. It is interesting to note that the majority of leached porphyrin exists in the free base form. Using Beer's law, the leeching of TPFPP was approximated as 2.3 mg per 1 g of product formed. At a catalyst loading of 18 $mg.g^{-1}$ this corresponds to approximately 5% of photosensitizer lost per 1 g of product formed. Although no porphyrin bands are visible for the TPP system (expected at 414 nm for the free base form) the absorbance of the polymer byproduct was used to establish an upper limit of leeching of *ca.* 10 µg under the same conditions as for TPFPP. Taking catalyst loading into account, this corresponds to a maximum of 0.2 % of photosensitizer lost per 1 g of product formed; however, it should be noted that the actual amount of photosensitizer lost is likely significantly lower.

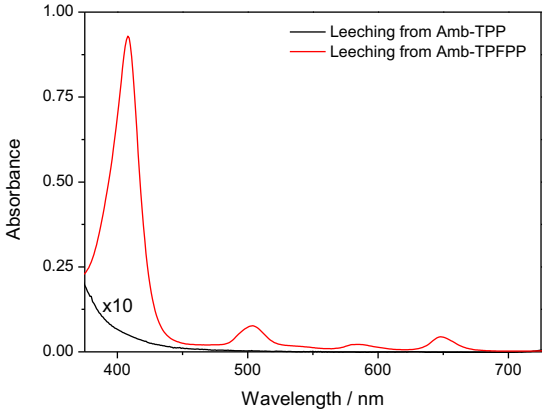

Figure S6: UV-visible spectroscopy of crude products following flow experiments using the system of photocatalyst bound to Amberlyst-15 measured at a pathlength of 1 cm. In both cases the same amount of product was dissolved in ethyl acetate and measured at a pathlength of 1 cm. **Red**: The Amb-TPFPP system (Entry 6 in Table S2). **Black**: The Amb-TPP system; the y-axis is multiplied by 10 for clarity (Entry 11 in Table S2).

5. Batch synthesis of artemisinin in aqueous mixtures

4.1. Equipment for carrying batch photo-oxidation experiments

Batch photo-oxidation reactions are carried out in a three-necked flask, equipped with a magnetic stirrer, a reflux condenser. A thermometer and a gas inlet tube extend into the lower half of the flask. The gas inlet tube is attached to the inlet tube of a gas-washing bottle which serves as a safety trap to prevent liquid from being drawn into the oxygen source. The gas-washing bottle is connected to a commercial cylinder of oxygen (BOC) and maintains a continuous stream of gas. Photolysis is carried out with one or two (symmetrically positioned on each side of the reactor) banks of LED lamps.

4.2. Temperature selectivity study of the Schenk ene reaction at 30 ºC and at -10 ºC

In a 2 necked round bottom flask, **3** (250 mg, 1.06 mmol) and a suitable photosensitizer (0.7 mg, 0.001 mmol) are dissolved in 20 mL of 4:1 ethanol:water. The reaction mixture is heated to 30 ºC using an oil-bath or cooled to -10 ºC using a cooling bath. Internal reaction temperature is monitored using a thermocouple. In case of heating, an additional reflux condenser is added to prevent partial evaporation of the solvent. The solution is oxygenated by continuous bubbling of O_2 at atmospheric pressure. The flask is irradiated with LED lamps for 6 hours. The conversion and selectivity to the desired isomer are monitored by ^{1}H NMR by taking regular aliquots concentrated under high vacuum.

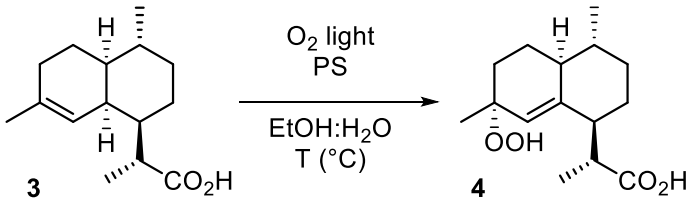

Table S3: Solvent, photosensitizer and acid conditions screening.

Entry	Solvent	vol:vol	PS	T (ºC)	Conversion	Selectivity (4:5)
1	EtOH:H_2O	80:20	$[Ru(bpy)_3]Cl_2$	-10	>98%	87:13
2	EtOH:H_2O	80:20	$[Ru(bpy)_3]Cl_2$	30	>98%	87:13

^{1}H-NMR spectra are acquired in acetone-d_6 to avoid decomposition of the hydroperoxide and overlapping of the isomers peaks. Vinylic hydrogen of tertiary hydroperoxide **4** is seen at δ = 5.30 ppm; vinylic hydrogens of secondary hydroperoxide **5** are seen at δ = 5.12 and 4.82 ppm.

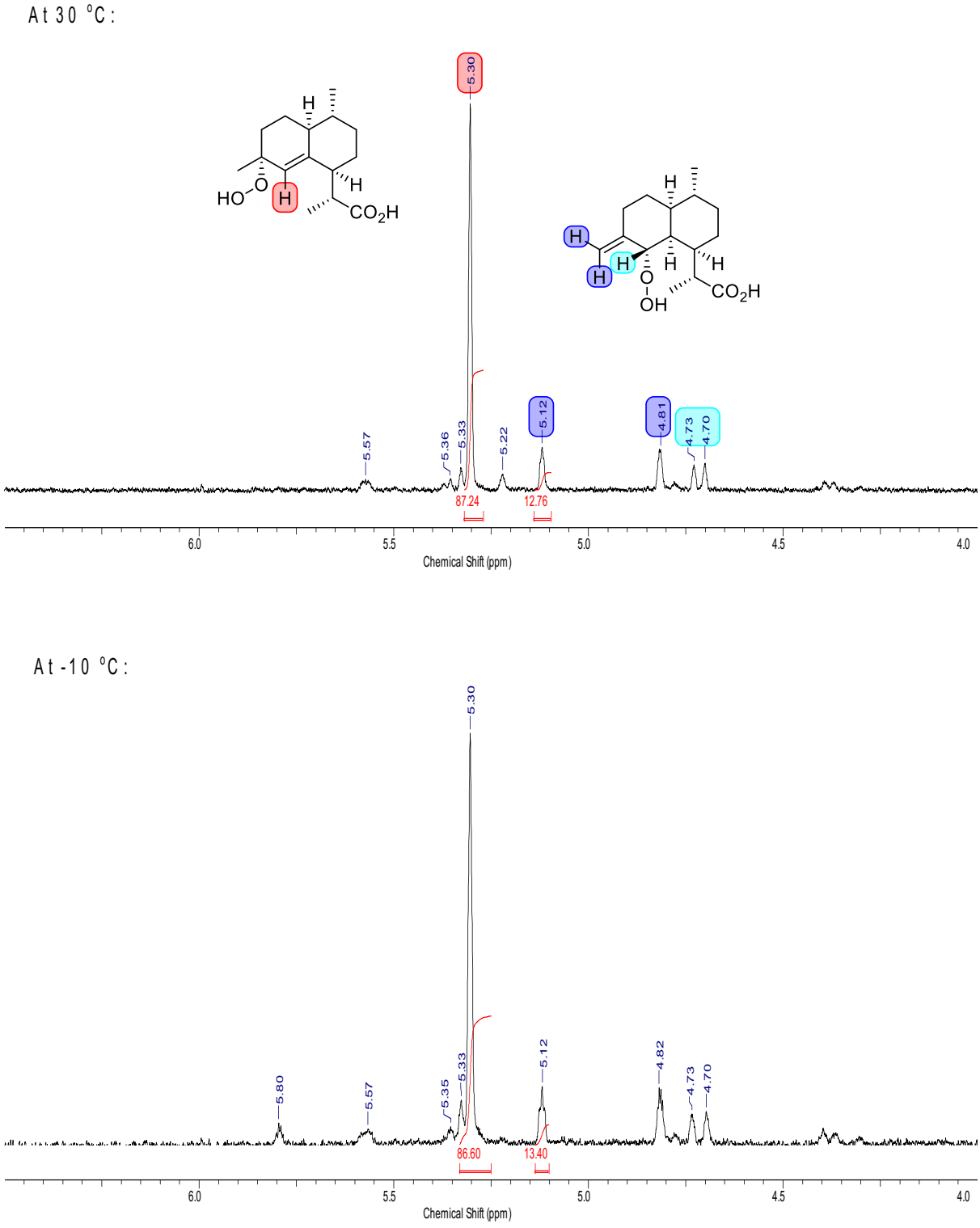

Figure S7: A zoomed in 1H NMR in acetone-d_6 after photo-oxidation of **3** in ethanol:water mixtures at 30 and -10 ºC showing the relevant vinylic H groups from the different isomers. The 2 isomers generated in reasonable quantity (**4** and **5**) are highlighted in color.

4.3. One pot batch procedure in dichloromethane (control experiment Table S4, entry 1)

3 (250 mg, 1.06 mmol), biphenyl (163 mg, 1.06 mmol) and tetraphenylporphyrin (0.6 mg. 0.001 mmol) are dissolved in dichloromethane (50 mL). The reaction mixture is cooled down to 0ºC in an ice-brine bath, trifluoroacetic acid (80 µL) is added dropwise under vigorous stirring and O_2 is slowly bubbled through the solution. The flask is irradiated with LED lamps for 2 hours. The conversion is monitored by ^{1}H NMR by taking regular aliquots and the mixture is allowed to warm up to room temperature and O_2 is kept bubbling continuously for another 5 hours. After removal of the volatiles, conversion and selectivity to **1** is measured by ^{1}H NMR in $CDCl_3$ using biphenyl as an internal standard.

4.4. One pot batch aqueous procedure for photo-sensitizer, solvent and acid screening: (Table S4, entries 2-16)

Various conditions for the one-pot synthesis of **1** from **3** (Scheme S5) were examined. Results are detailed in Table S4 below:

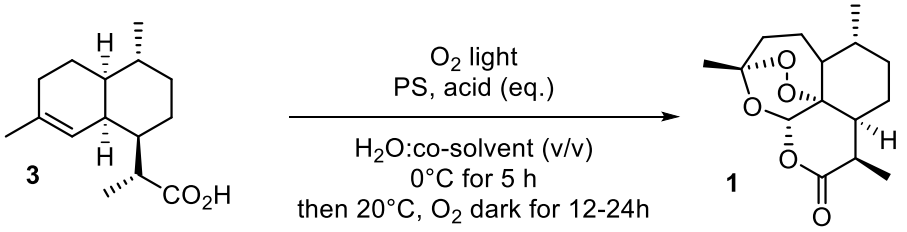

Scheme S5: General batch procedure used for solvent and photosensitizer screening.

3 (250 mg, 1.06 mmol) and the desired photosensitizer (0.001 mmol) are dissolved in the organic solvent first and then, diluted with freshly deionized water (V_{org}/V_{H2O} ratios are calculated to meet the required concentration). The reaction mixture is cooled to 0ºC, the acid is added dropwise under vigorous stirring and O_2 is bubbled through the liquid. The flask is irradiated with LED lamps for 5 hours (at 5-10°C). The conversion is monitored by ^{1}H NMR

by taking regular aliquots extracted with diethyl ether. Once the starting material is entirely consumed, the mixture is allowed to warm to room temperature and O_2 is kept bubbling continuously for another 24 hours. The organics are extracted with diethyl ether (3 x 100 mL). The organic layer is then washed with brine (100 mL) and dried over Na_2SO_4. After removal of the volatiles, conversion and selectivity to **1** is measured by ^1H NMR in $CDCl_3$ by adding 147 μL of mesitylene as an internal standard.

Table S4: Solvent, photosensitizer and acid conditions screening for the one-pot batch synthesis of artemisinin.

Entry	Solvent	vol:vol	[3] mol.L^{-1}	PS	Temp (°C)	Acid	Eq.	Conversion (%)[a]	Yield (%)[a]
1	DCM	100	2.1 x10^{-2}	TPP	10°C	TFA	0.5	100	54
2	PEG:H_2O	50:50	2.1 x 10^{-2}	RB	10°C	TFA	0.5	0	0
3	THF:H_2O	50:50	2.1 x10^{-2}	RB	10°C	TFA	0.5	> 98	< 5
4	THF:H_2O	60:40	5.3 x10^{-2}	RB	10°C	TFA	6.3	13	53
5	THF:H_2O	60:40	5.3 x10^{-2}	TPP	10°C	TFA	0.5	98	56
6	EtOH:H_2O	60:40	5.3 x10^{-2}	TPP	10°C	TFA	0.5	0	0
7	EtOH:H_2O	60:40	5.3 x10^{-2}	$[Ru(bpy)_3]Cl_2$	10°C	TFA	0.5	> 98	50
8	EtOH:H_2O	60:40	2.1 x10^{-2}	$[Ru(bpy)_3]Cl_2$	10°C	TFA	0.5	> 98	50
9	THF:H_2O	60:40	5.3 x 10^{-2}	$[Ru(bpy)_3]Cl_2$	0°C	H_3PO_4	0.5	> 98	52
10	EtOH:H_2O	60:40	5.3 x10^{-2}	$[Ru(bpy)_3]Cl_2$	10°C	TFA	1.0	> 98	55
11	THF:H_2O	60:40	5.3 x10^{-2}	$[Ru(bpy)_3]Cl_2$	10°C	TFA	0.5	> 98	66
12	THF:H_2O	60:40	5.3 x10^{-2}	$[Ru(bpy)_3]Cl_2$	30°C	TFA	0.5	> 98	59

12	THF:H_2O	60:40	5.3 x10^{-2}	$[Ru(bpy)_3]Cl_2$	10°C	TFA	6.3	> 98	58
13	EtOH:H_2O	50:50	2.1 x10^{-2}	$[Ru(bpy)_3]Cl_2$	10°C	TFA	1.0	> 98	43
14	EtOH:H_2O	50:50	2.1 x10^{-2}	$[Ru(bpy)_3]Cl_2$	10°C	H_2SO_4	1.0	> 98	40
15	EtOH:H_2O	60:40	2.1 x 10^{-2}	$[Ru(bpy)_3]Cl_2$	10°C	H_2SO_4	0.5	> 98	47
16[b]	EtOH:H_2O	80:20	1.7 x 10^{-1}	$[Ru(bpy)_3]Cl_2$	0°C	H_2SO_4	0.5	> 98	50[c]
17	EtOH:H_2O	80:20	5.3 x 10^{-2}	$[Ru(bpy)_3]Cl_2$	30°C	H_2SO_4	0.5	> 98	39
18	^{i}PrOH:H_2O	60:40	5.3 x 10^{-2}	$[Ru(bpy)_3]Cl_2$	0°C	TFA	0.5	> 98	59
19	THF:EtOH:H_2O	5:75:20	2.1 x 10^{-2}	$[Ru(bpy)_3]Cl_2$	10°C	TFA	0.5	> 98	62
20	EtOH:H_2O	60:40	2.1 x 10^{-2}	TMPyP	10°C	H_2SO_4	0.5	> 98	53

[a] Conversion and yields are obtained by ^{1}H NMR analysis. [b] Reaction is conducted on a 6 g (0.025 mol) scale using 10 mg of photosensitizer in 150 mL solvent volume. Photo-irradiation was carried out for 8 hours at 0°C. [c] Yield is measured by adding 3.53 mL (0.025 mol) of mesitylene after extraction and evaporation of the volatiles.

4.5. Procedure for the gram scale batch artemisinin synthesis with recycling of the aqueous phase

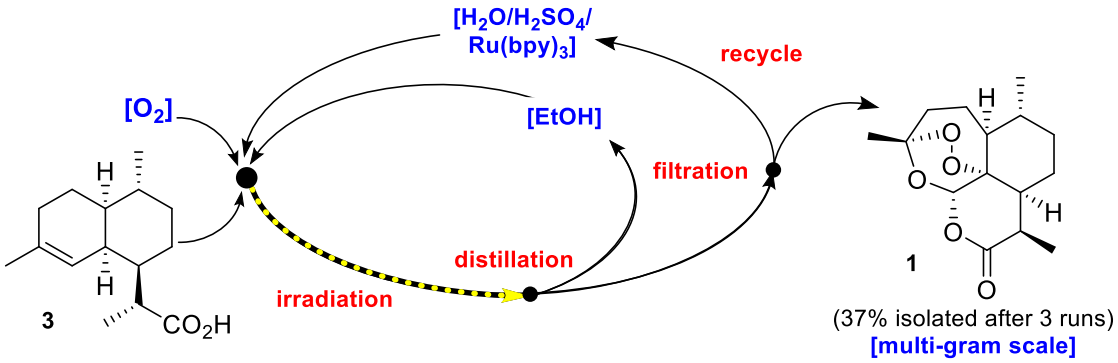

Scheme S6: Synthesis of **1** in batch using recycled acid and photocatalysts.

First reaction cycle:

The recycling of acid and photocatalyst is summarized in Scheme S6. A 500 mL three-necked flask is charged with **3** (1.0 g, 4.24 mmol) which is dissolved in ethanol (120 mL, 8.3 $g.L^{-1}$). The solution is then diluted with freshly deionized water to a total volume of 200 mL (60/40 V_{EtOH}/V_{H2O}, 5.0 $g.L^{-1}$). The hexahydrate of $[Ru(bpy)_3]Cl_2$ (10 mg, 0.013 mmol) is added and the reaction mixture is immersed in an ice bath to allow cooling to 0°C (internal temperature). Once the reaction temperature is reached, sulfuric acid (112 µL, 0.5 eq) is added dropwise under vigorous stirring and the solution is oxygenated by continuous oxygen bubbling. The mixture is irradiated for 9 hours after which the oxygenation is allowed to continue for 24 hours. The reaction is monitored by ^1H NMR in $CDCl_3$ by taking regular aliquots (0.3 mL). After a total reaction time of 33 hours, ethanol is removed from the crude mixture by heating to 50 °C under reduced pressure until a white precipitate is observed. The mixture is allowed to cool to room temperature under air and to sit overnight. White crystalline needles of **1** are recovered by filtration and washed with deionized water (40 mL) (see Figure S9). The crystals are dried under vacuum and ^1H NMR analysis revealed over 98% purity at this stage. More product (m= 450 mg) can be isolated by fractional crystallization from the aqueous mother liquor with the same purity.

Second reaction cycle:

A new reaction batch is prepared to recycle the liquid phases, including ethanol, the combined aqueous mother liquor and the washings. **3** (1.5 g) is dissolved in used and fresh ethanol (V_{tot} = 180 mL). The mixture is diluted with the mother liquor (V = 120 mL) and the reaction is carried out using the same set up as previously described. Irradiation is maintained for 10 hours and conversion is monitored by ^{1}H NMR in $CDCl_3$. After a total reaction time of 35 hours, the crude mixture is purified as described above, using 45 mL of deionized water (m= 690 mg of isolated product).

Third recycling:

3 (2.2 g) is dissolved with used and fresh ethanol (V_{tot} = 263 mL). The mixture is diluted with the mother liquor (V_{tot} = 175 mL) and the reaction is carried out using the same set up as previously described. Irradiation is maintained for 17 hours and conversion is monitored by ^{1}H NMR. After a total reaction time of 48 hours, the crude mixture is purified as described above, using 50 mL of deionized water (m = 954 mg).

Table S5: Recycling of the mother liquor

Aqueous Solution	H_2O + H_2SO_4	H_2O + H_2SO_4 + $Ru(bpy)_3$	mother liquor after the 1st pass	mother liquor after the 2nd pass	mother liquor after the 3rd pass
pH	1.58	1.51	1.63	1.92	2.25
Mass			450 mg	690 mg	954 mg
Artemisinin Purity (measured by ^{1}H NMR)			> 98 %	> 98 %	> 98 %

The isolated solid materials are combined (m_{tot}= 2.094 g, 37% isolated yield). The ^{1}H NMR spectra is recorded in $CDCl_3$ to observe exclusively the desired product **1**, which is identical to

natural (+)-artemisinin: m.p. 155-6°C, (Sanofi product 158-9°C); $[\alpha]_D^{25}$ +66.7 (*c* 1, $CHCl_3$), (Sanofi product +66.8 (*c* 1, $CHCl_3$).

Figure S8: Crude **1** isolated after filtration and aqueous washing. The water soluble photo and acid-catalysts remain in the aqueous solution.

5. Continuous flow experiments in aqueous mixtures

5.1. High Pressure Continuous Flow Equipment

Continuous flow experiments involving aqueous mixtures are performed using a modified version of the high pressure photo-oxidation reactor and equipment as described above (see Figures S3 and S10). The reactor system is operated in *upflow* mode such that the flow rates of O_2 and the solution of **3** are essentially independent and, in each experiment, the feed solution is saturated with O_2 prior to use. Glass balls (6 mm) are loaded into the sapphire tube (Saint-Gobain crystals, 10 mm o.d., 120 mm long, 1 mm wall thickness) so as to reduce inner filter effects upon irradiation by reducing the path length.

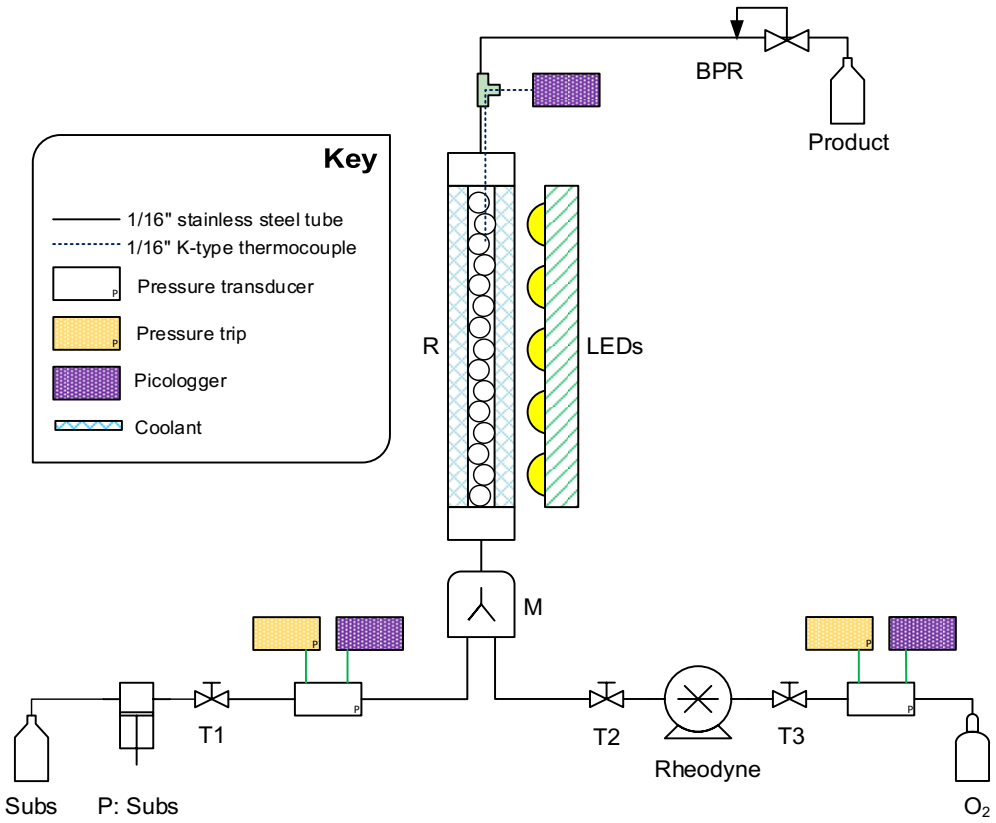

Figure S9: Reactor schematic for the flow synthesis of **1**, using an aqueous mixture as the reaction solvent. **Subs**: **3** dissolved in the aqueous solvent system, with $[Ru(bpy)_3]Cl_2$ as photosensitizer and H_2SO_4 as the homogenous acid, which is pumped by **P:Org 1** (a Jasco™ PU-980 HPLC pump); O_2 is added using a modified **Rheodyne** dosage unit. **M**: micromixer (IMM, Mainz) to allow thorough mixing of the aqueous solution and O_2; **R**: sapphire tube reactor which is temperature controlled *via* a circulating water/ethylene glycol bath and filled with glass balls (6 mm); **LEDs**: light source (3 × 5 × Citizen Electronics Co. Ltd CL-L233-C13 N mounted on water cooled

stainless steel blocks); **BPR**: back pressure regulator (model Jasco™ BP 1580-81); **T*N***: (where N is a number) manual valve.

5.2. Adjustments of the reaction parameters for photo-oxygenation

Various conditions for the photo-oxidation of **3** to **1** are examined (Scheme S7). The relevant results are detailed in Table S5.

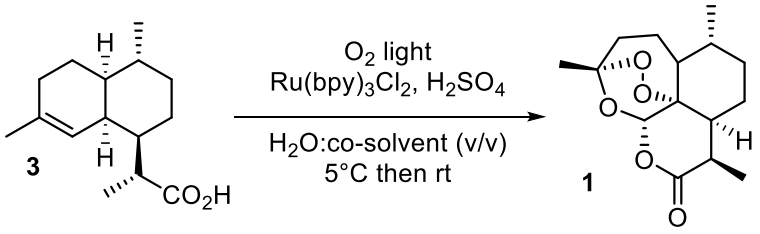

Scheme S7: General procedure used for solvent and photosensitizer optimization.

3 is dissolved in the organic solvent first and the solution is diluted with freshly deionized water (V_{org}/V_{H2O} ratio are calculated to meet the required concentration). $[Ru(bpy)_3]Cl_2$ and H_2SO_4 (> 95%, 0.56 µL per mL of solution) are then added to the mixture. This solution is subsequently pumped and mixed with O_2 in a micro mixer **M** (Figure S10), and irradiated in the photoreactor at 5 °C. The product is collected at the outlet of the BPR and analyzed with no further work up. To calculate reaction conversion, 1 mL of the product solution is collected directly from the photoreactor, the solvent is removed under vacuum and 1 equivalent of mesitylene is added prior to obtaining the ^{1}H-NMR spectrum. The conversion of **3** is obtained relative to the relevant peak corresponding to mesitylene and the results are presented in Table S5.

To calculate the yields of **1**, aliquots (1 mL) are collected after the photoreactor and allowed to warm up to room temperature under air for an additional 24 hours. Then, the solvent is removed under vacuum and an equivalent of mesitylene is added prior to analysis by ^{1}H-NMR in $CDCl_3$. Additional experiments have been conducted using THF as a co-solvent. For experiment entry 32 Table S5, the stream was collected from the photoreactor in a stainless steel autoclave at 10 bar O_2 for *ca.* 16 hours.

Table S6: results for the flow synthesis of artemisinin in aqueous mixtures

Entry	Solvent	Solvent Ratio vol:vol	[**3**] mol.L^{-1}	[PS] mol.L^{-1}	Pressure (bar)	Flow rate mL.min^{-1}	Conversion of **3** NMR (%)	Yield of **1** NMR (%)
1	EtOH:H_2O	60:40	0.02	1.0 x 10^{-4}	1	0.25	99	N/A
2						0.50	93	
3						2.00	69	
4	EtOH:H_2O	60:40	0.02	**2.0 x 10^{-4}**	1	0.25	99	38
5						0.50	96	
6						1.00	80	
7						2.00	69	
8	EtOH:H_2O	60:40	0.02	1.0 x 10^{-4}	**10**	0.50	100	28
9						1.00	96	
10						2.00	90	
11						4.00	68	
12						0.25	96	29
13						0.50	90	

14	EtOH:H_2O	**80:20**	0.02	1.0 x 10^{-4}	1	1.00	84	
15						2.00	80	
16						4.00	38	
17	EtOH:H_2O	80:20	**0.04**	1.0 x 10^{-4}	1	0.25	94	23
18						0.50	67	
19						1.00	61	
20						2.00	43	
21						4.00	33	
22	EtOH:H_2O	80:20	0.04	1.0 x 10^{-4}	**10**	0.25	98	21
23						0.50	98	
24						1.00	93	
25						2.00	77	
26						4.00	56	
27	**EtOH:H_2O:THF**	75:20:5	0.02	1.0 x 10^{-4}	10	0.25	99	46
28						0.50	98	
29						1.00	96	

30						2.00	92	
31						4.00	54	
For the following experiment, the sample was left under a 10 bar pressure of oxygen for a further 16 hours, in a stainless steel vessel, prior to analysis								
32	**EtOH:H_2O:THF**	75:20:5	0.02	1.0×10^{-4}	10	0.25	99	16
33	**THF:H_2O**	60:40	0.21	1.0×10^{-4}	1	0.12	98	38
						0.25	92	
						0.50	87	
34	**THF:H_2O**	60:40	0.21	1.0×10^{-4}	10	0.12	98	36
						0.25	98	
						0.50	90	

[a] Conversion and yields are obtained by ^{1}H NMR in $CDCl_3$ in comparison to mesitylene as an internal standard

6. Green Metrics Calculations

The E-Factors presented were calculated using Sheldon's approach,[39] who defined the E-Factor as the ratio of the mass of waste produced over the mass of product obtained (equation 1). The side-products (SP) produced are assumed to possess the same molecular weight as the starting material (SM).

$$E\ factor = \frac{Mass\ of\ waste}{Mass\ of\ product} \quad (1)$$

Separate E-Factor values, including (*E factor* 1) or excluding (*E factor* 2) the mass of the reaction solvent, are calculated. For all processes the masses of components of the as-performed reactions were initially determined and then normalised to 1 kg of artemisinin product. These are summarised in Table S7.

1. In the Sanofi process, the calculated values include the mass of waste obtained from the activation step and the photo-oxygenation step. The mass of the side-product was calculated as $m(\mathrm{SP}) = m(\mathrm{SM})/(1 - yield)$. The data have been obtained from reference 10.
    - For the activation step: we take into account the masses of HCl, EtOH and CO_2 generated as well as the base (K_2CO_3) used.
    - For the photo-oxygenation step: we take into account the mass of acid (TFA), photocatalyst (TPP) and base (Na_2CO_3).
    - The mass of solvent (DCM) calculated includes both steps as this is a one pot process. Recrystallization solvents (Heptane and EtOH) and charcoal used for purification are also taken into account.

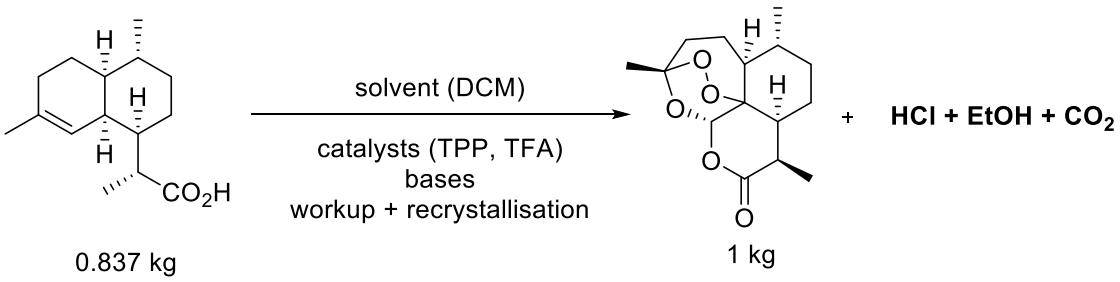

Theoretical E Factor (100% yield)

$$\text{E Factor} = \frac{36 + 46 + 44}{282} = 0.45$$

Experimental E Factor

$$\text{E Factor 1} = \frac{m(\text{SP}) + m(\text{HCl}) + m(\text{Cat}) + m(\text{Bases}) + m(\text{Charcoal}) + m(\text{Solvents})}{m(\text{Prod})}$$

$$\text{E Factor 2} = \frac{m(\text{SP}) + m(\text{HCl}) + m(\text{Cat}) + m(\text{Bases}) + m(\text{Charcoal})}{m(\text{Prod})}$$

Scheme S8: E-Factor calculations for the Sanofi process.

2. In our processes, namely the heterogeneous bi-functional catalysis in liquid CO_2 (strategy 1) and the binary aqueous solvent system (strategy 2), the calculated values include the mass of waste obtained from the photo-oxygenation step. This takes into account the amounts of acid catalyst (solid or homogeneous), the organic solvents and the photocatalysts (TPP or $Ru(bpy)_3Cl_2$). As above, the masses of the side-products have been calculated as $m(\text{SP}) = m(\text{SM})/(1 - yield)$.
   - The CO_2 process values have been obtained from table S2 entry 11 (short reactor) and entry 12 (long reactor) in Section 4.5 in the supplementary information.
   - The values for the EtOH/H_2O processes have been obtained from the reaction described in Section 4.5 in the supplementary information. For the process involving three cycles we have considered the total amount of product and waste produced over all cycles. The values for the THF/H_2O process have been obtained from Entry 11, Table S4. In this experiment, the isolated yield is estimated.

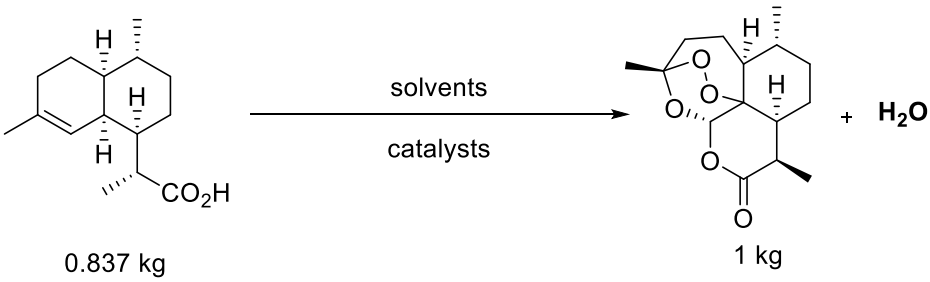

0.837 kg

1 kg

Theoretical E Factor (100% yield)

$$\text{E Factor} = \frac{0}{282} = 0$$

Experimental E Factors

$$\text{E Factor 1} = \frac{m(\text{SP}) + m(\text{Cat}) + m(\text{Solvents})}{m(\text{Prod})}$$

$$\text{E Factor 2} = \frac{m(\text{SP}) + m(\text{Cat})}{m(\text{Prod})}$$

Scheme S9: E-Factor calculations for the CO_2 and EtOH/H_2O processes.

Table S7: E-factor metrics and calculations

Process	Yield	3 (kg)	Acid	PS	Solvent 1	Solvent 2	Solvent 3	Solvent 4	Purifying agents	Additive 1	Additive 2		E1	E2
Sanofi			**TFA**	**TPP**	**CH_2Cl_2**	**Hep**	**EtOH**	**H_2O**	**Na_2CO_3**	**Charcoal**	**(HCl +EtOH+CO_2)**	**K_2CO_3**		
	55%	1.52	0.335	0.001	16.7	12.6	0.838	9.31	1.83	0.077	0.260+0.329+0.903	1.04	**36**	**4.8**
Strategy 1			**Amb**	**TPP**	**Tol**	**CO_2**								
4 cycles (short tube)	39%	2.15	6.4	0.215	15	74							**23 (97)* [31]****	**8**
1 cycle (long tube)	39%	2.15	12.9	0.429	15	74							**30 (104)* [37]****	**15**
Strategy 2 (EtOH/H_2O)			**H_2SO_4**	**$[Ru(bpy)_3]^{2+}$**	**EtOH**	**H_2O**								
1 cycle	38%	2.20	0.457	0.022	209	176							**210**	**1.8**
3 cycles	37%	2.26	0.100	0.005	100	38							**101**	**1.5**
Strategy 2 (THF/H_2O)			**TFA**	**$[Ru(bpy)_3]^{2+}$**	**THF**	**H_2O**								
1 cycle	50%	1.67	0.404	0.007	71	54							**73**	**1.3**

* Taking CO_2 into account ** Taking 10% CO_2 into account (assumed lost during recycle)

6. Characterization and spectral data for a sample of 1 isolated under conditions in Table S4, entry 16 and comparison with an authentic sample of 1 from the commercial process.

Melting point = 155-156 ºC; commercial sample (measured in Nottingham) 158-159 ºC.

$[\alpha]_D$ = +66.7º (c = 1,$CHCl_3$); commercial sample (measured in Nottingham) +66.8º

^{1}H NMR (300 MHz, $CDCl_3$): δ 5.87 (s, 1H), 3.41 (dq, *J* = 7.3, 5.4 Hz, 1H), 2.44 (td, 1H), 2.09–1.98 (m, 2H), 1.91–1.86 (m, 1H), 1.81–1.74 (m, 2H), 1.56–1.34 (m, 3H), 1.46 (s, 3H), 1.22 (d, *J* = 7.3 Hz, 3H), 1.11–1.04 (m, 2H), 1.01 ppm (d, *J* = 6.0 Hz, 3H). ^{13}C NMR (125 MHz, $CDCl_3$): δ 172.1, 105.4, 93.7, 79.5, 50.1, 45.0, 37.5, 36.0, 33.6, 32.9, 25.2, 24.9, 23.4, 19.8, 12.5 ppm. IR (KBr): ~n= 3455, 2954, 2850, 1733, 1456, 1384, 1199, 1113, 1027, 992 cm^1. HRMS calcd for $C_{15}H_{23}O_5$, $[M+H]^+$ 283.1540, found 282.1518. In agreement with commercial artemisinin sample and published data (ref 10).

^{1}H NMR (zoomed in spectra) of commercial (red) and synthesized artemisinin (blue).

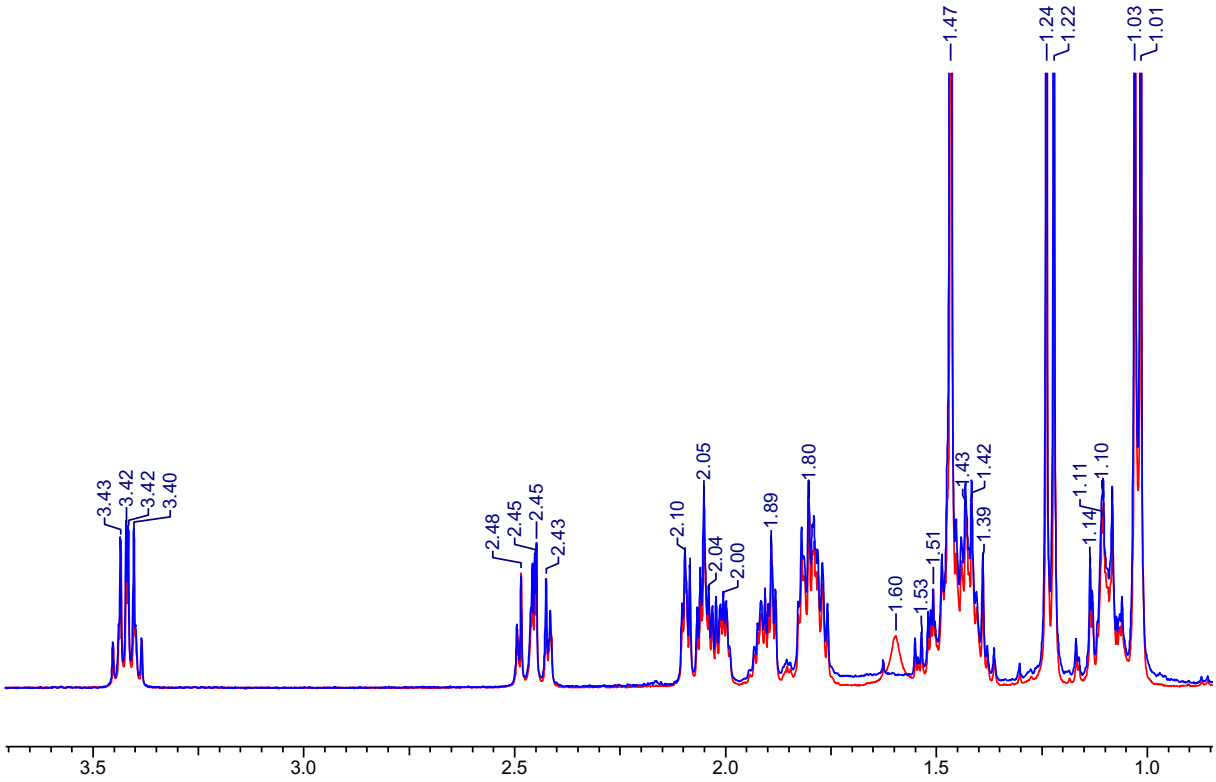

The same ^{1}H NMR spectra but with greater zoom of commercial (1) and synthesized artemisinin (2).

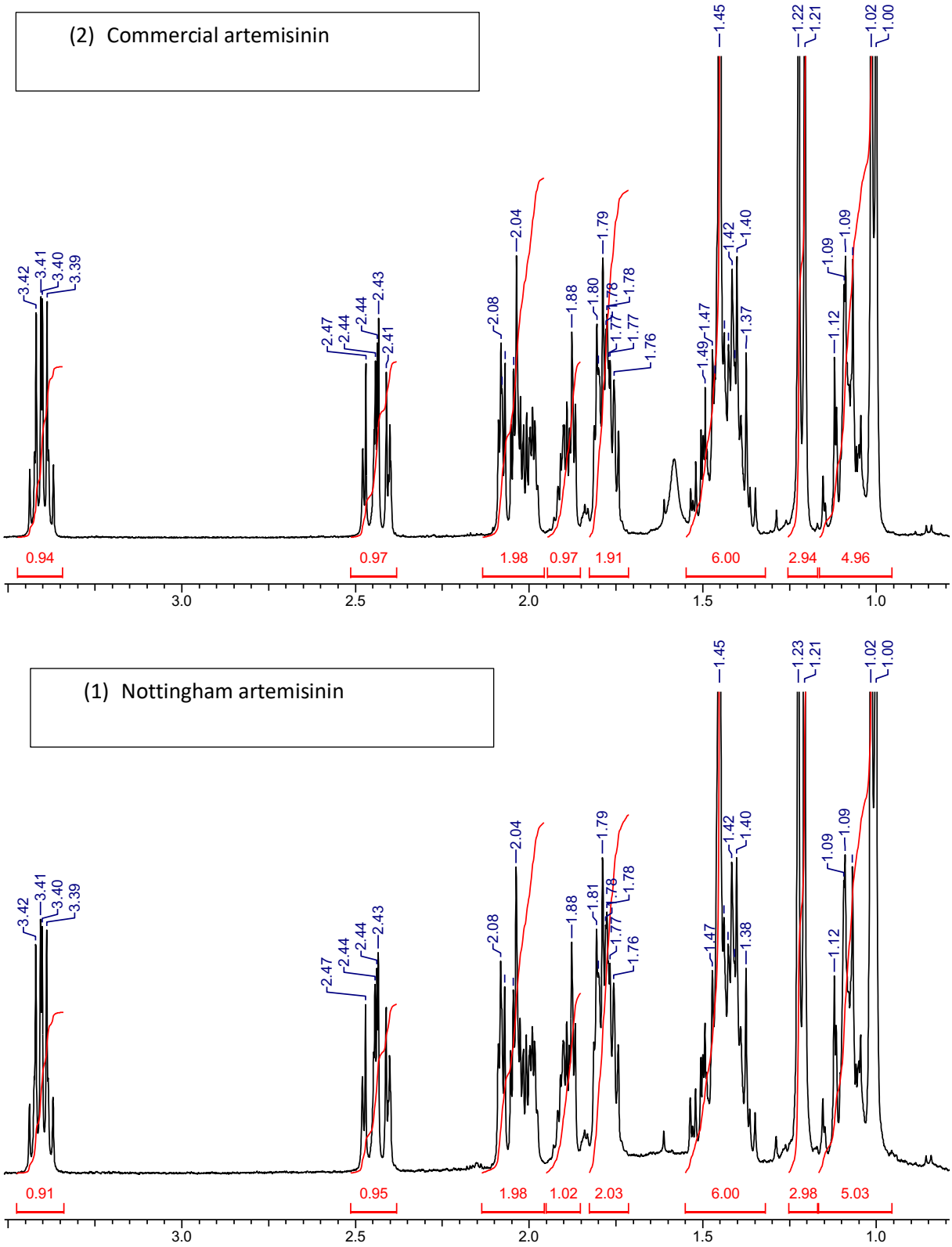

The full range of these ^{1}H NMR spectra of commercial and synthesized artemisinin.

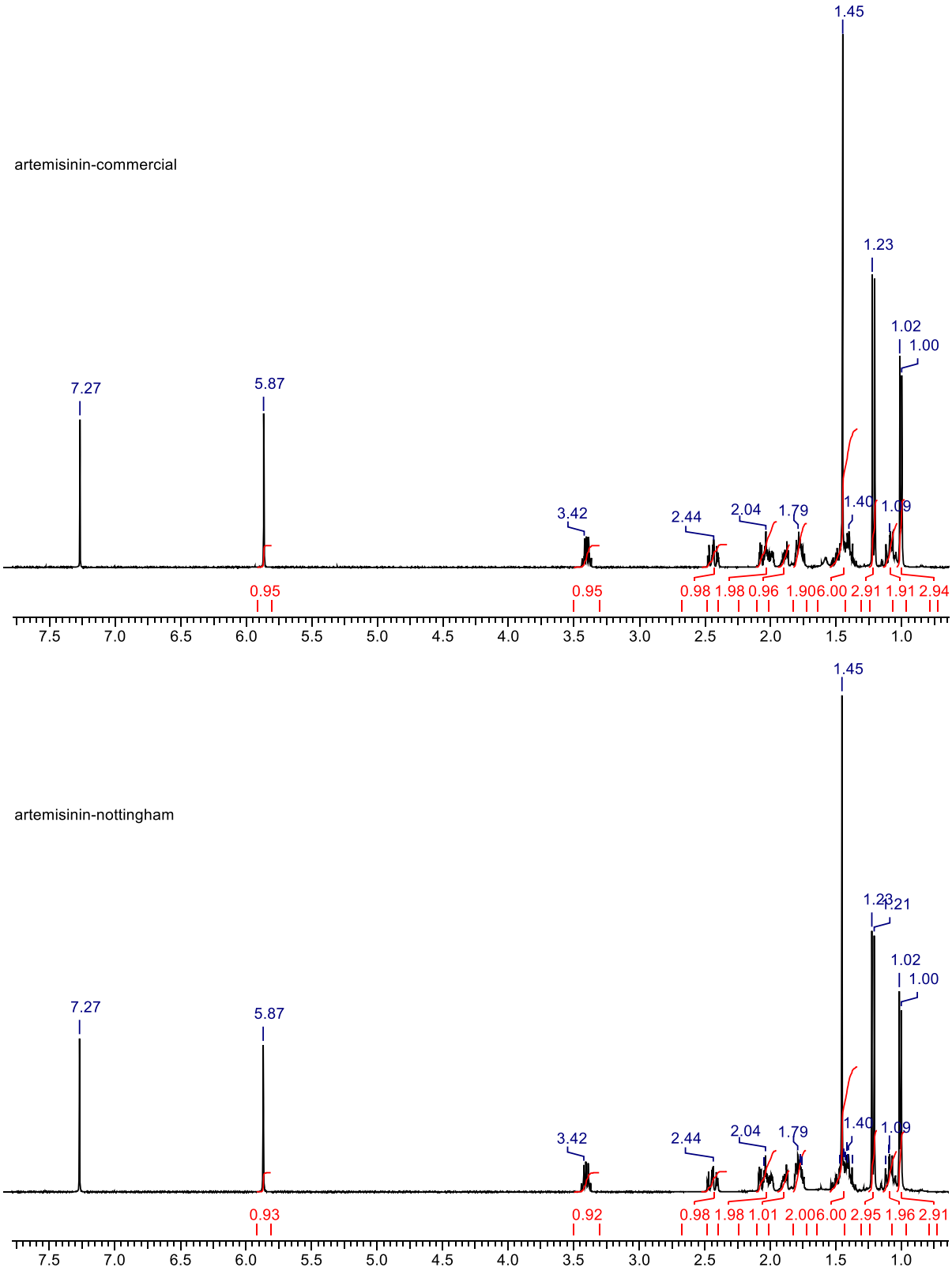

Crude ^{1}H NMR after removal of toluene from the fourth pass the continuous flow synthesis of 1 in CO_2, as shown in Table S2, entry 11. Mesitylene is used as an internal standard (1.0 eq.).

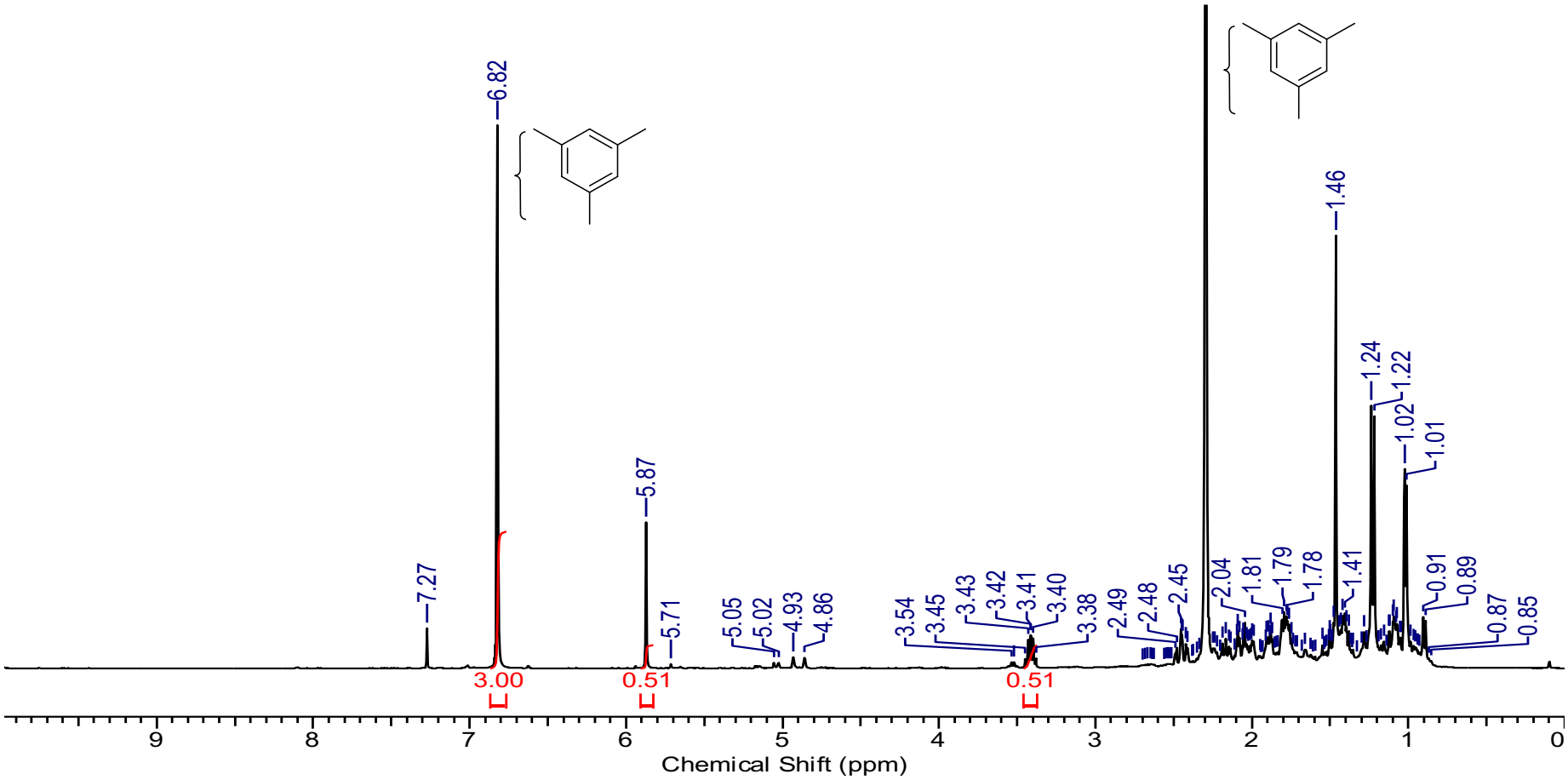

Crude ^{1}H NMR (400MHz, $CDCl_3$) after removal of volatiles with reaction conditions shown in Table S4, entry 11 (THF:H_2O 60:40). Biphenyl is used as an internal standard (0.1 eq).

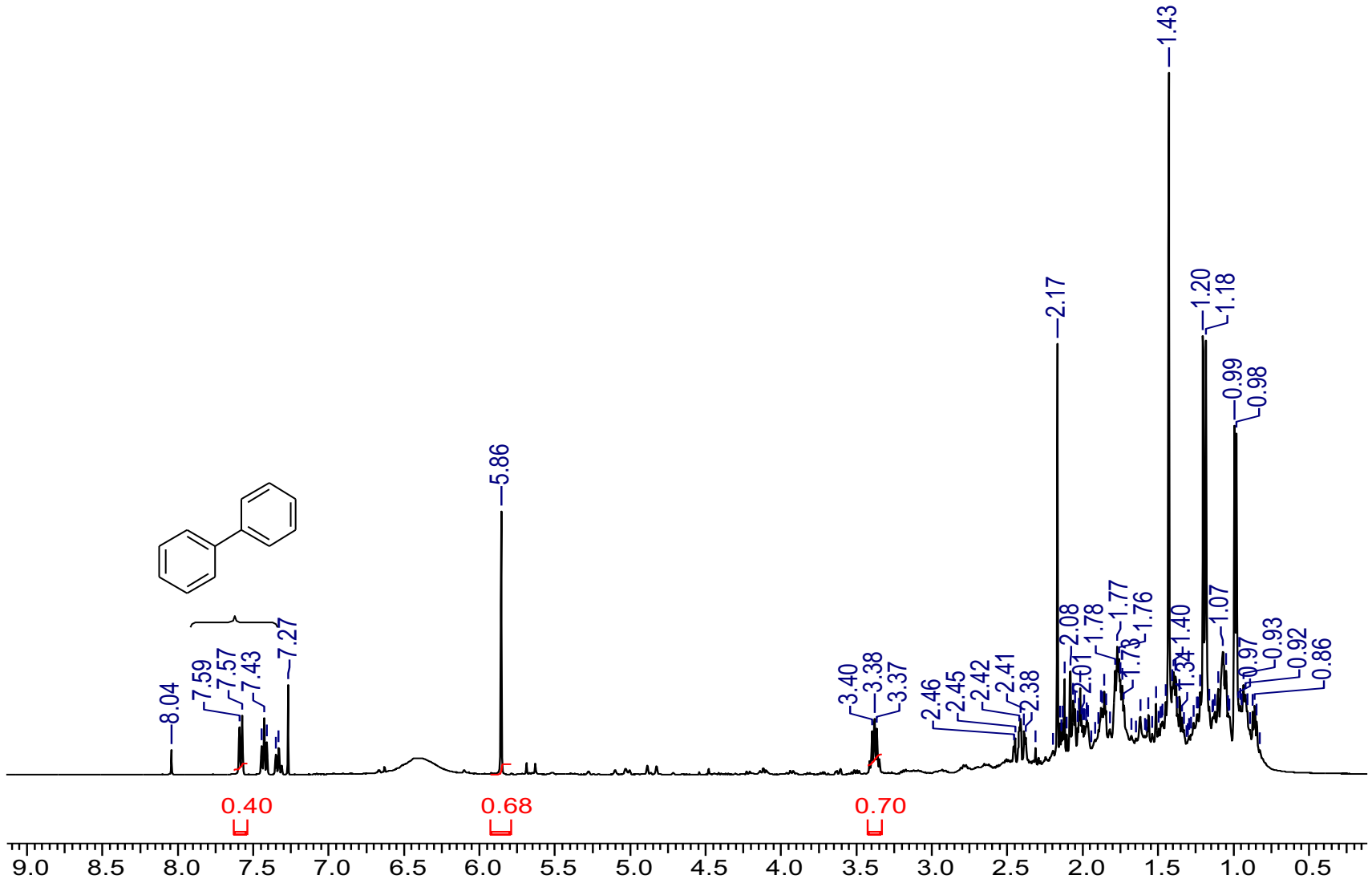

Crude ^{13}C NMR (125MHz, $CDCl_3$) after removal of volatiles with reaction conditions shown in Table S4, entry 11 (THF:H_2O 60:40). Biphenyl is used as an internal standard (0.1 eq).

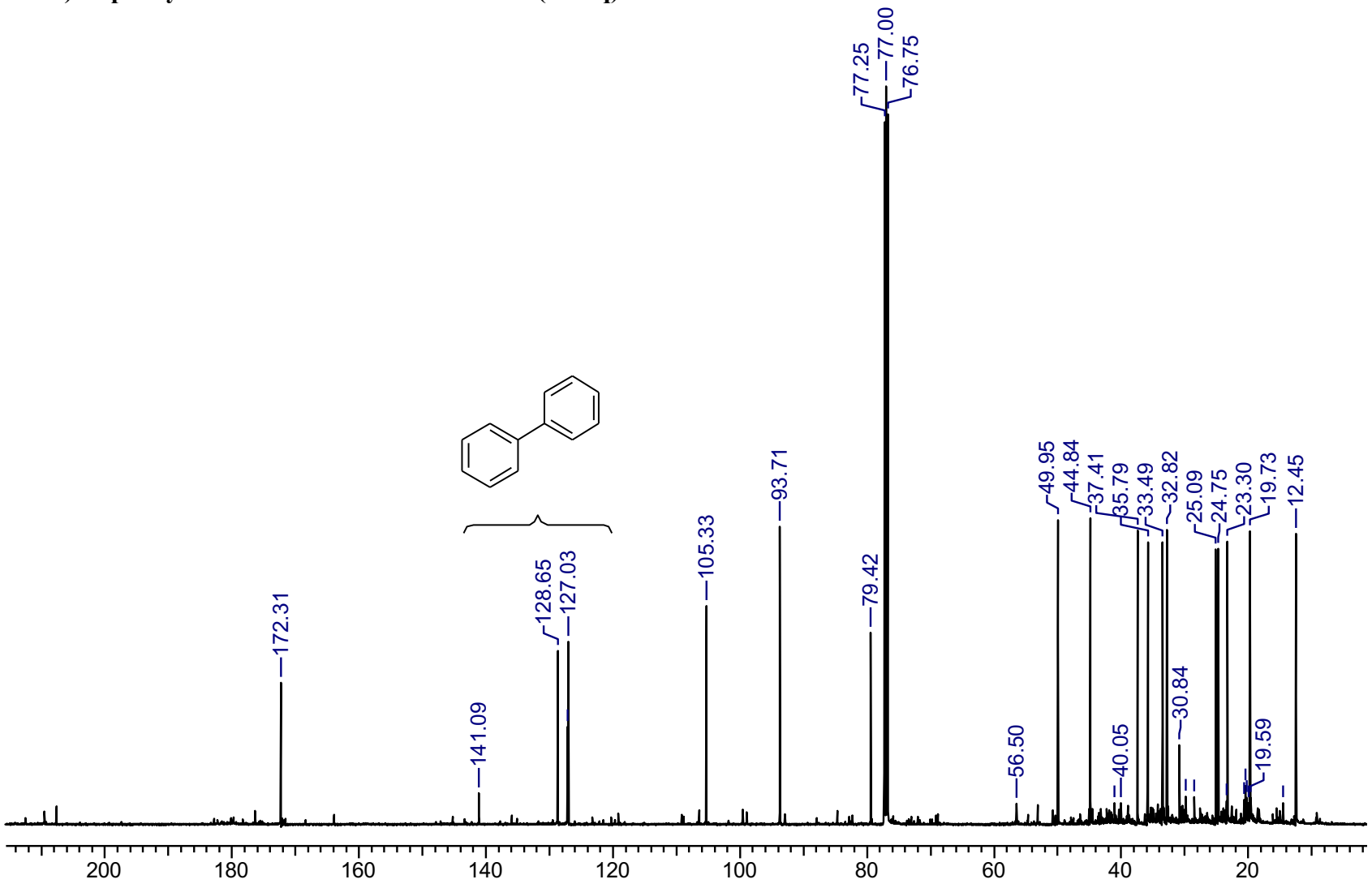

Crude ^{1}H NMR (300 MHz, $CDCl_3$) of artemisinin 1 isolated after slow air evaporation of the ethanol at room temperature and filtration of the reaction mixture (Table S4 entry 16). Mesitylene was added as an internal standard (1.0 eq.)

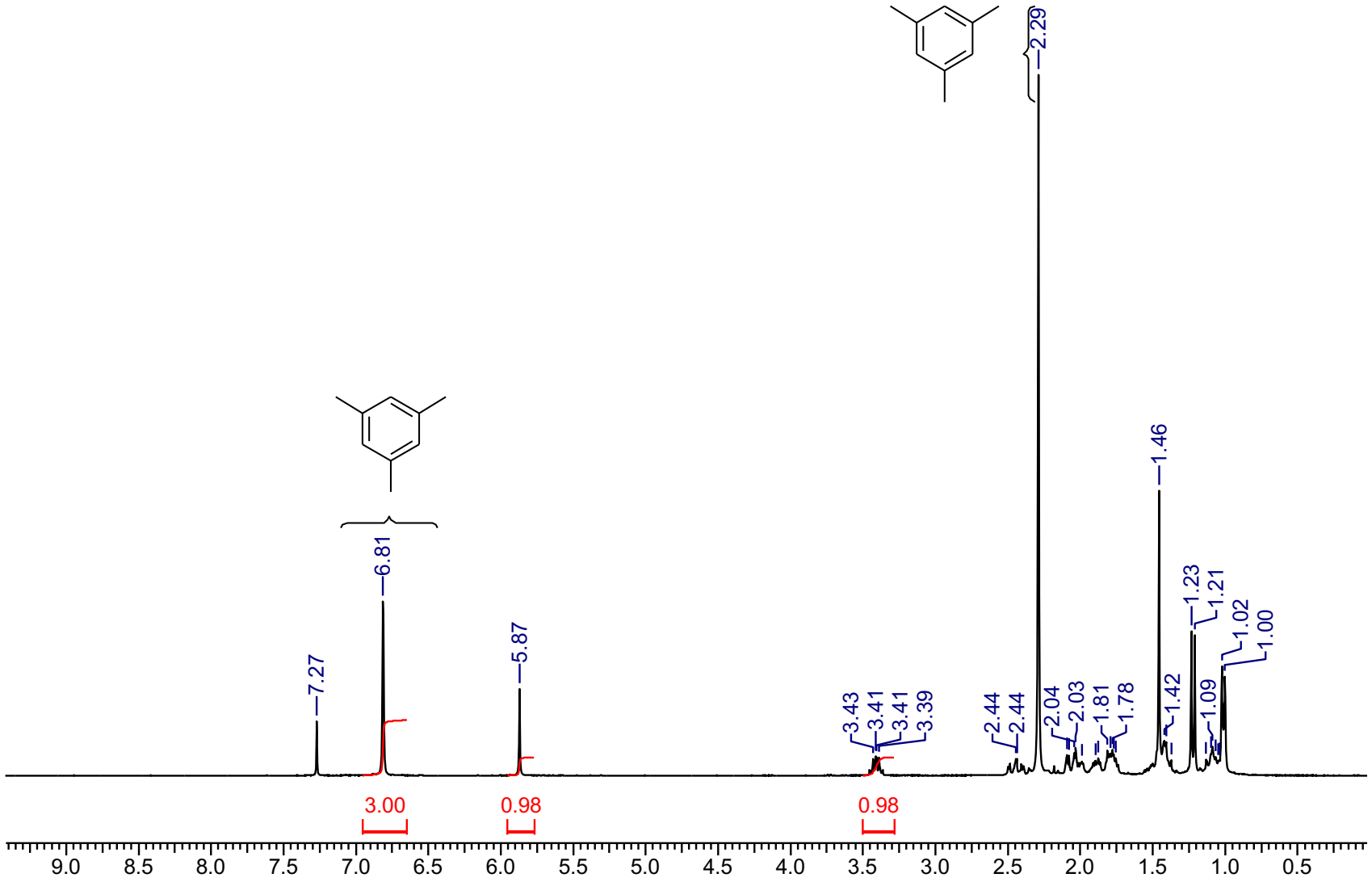

^{13}C NMR (125 MHz, $CDCl_3$) of artemisinin isolated after slow air/room temp. evaporation of the ethanol and filtration of the reaction mixture EtOH:H_2O (60:40) Table S4 entry 16.

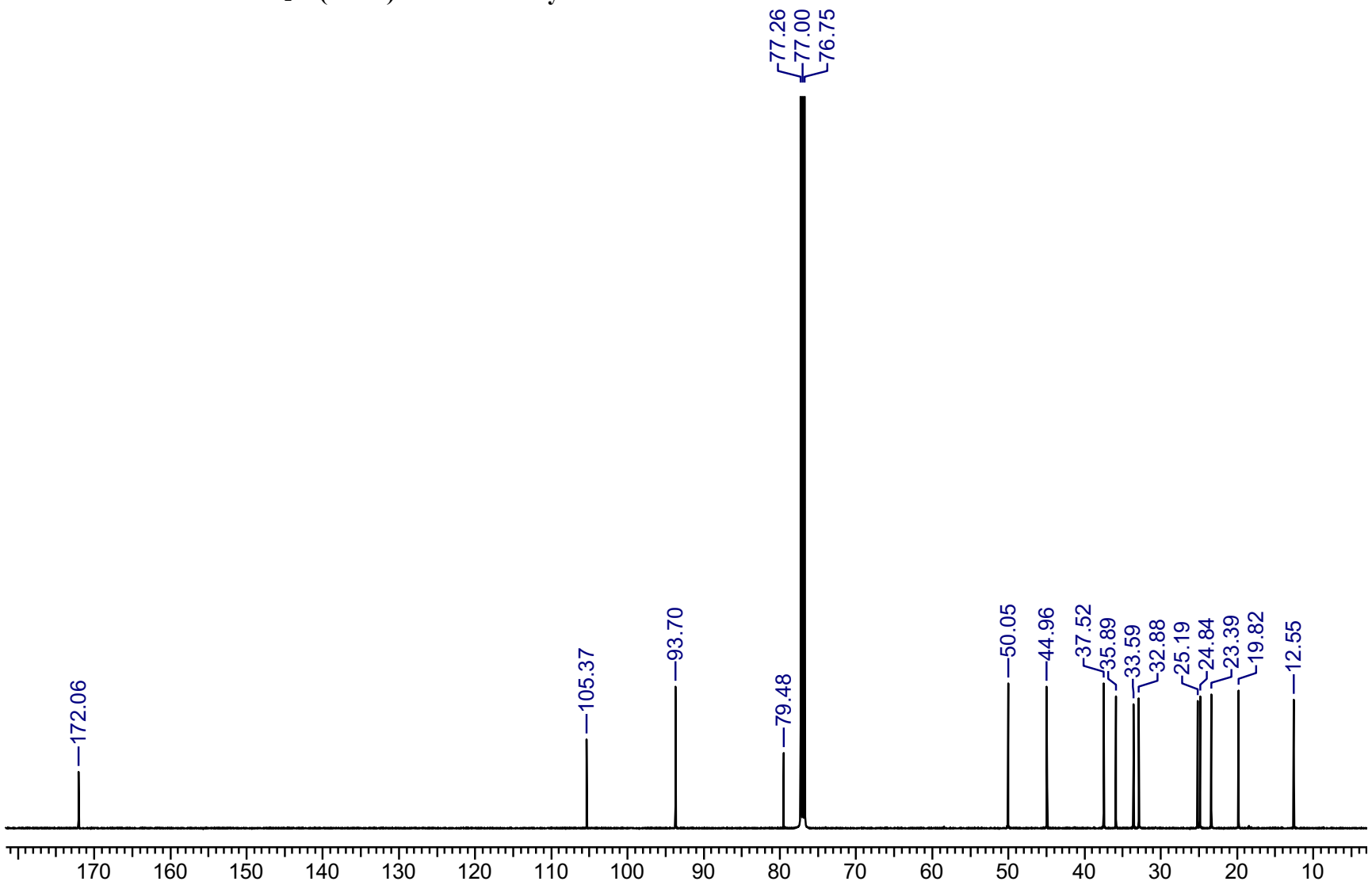

IR spectrum of artemisinin isolated after slow air/room temp. evaporation of the ethanol and filtration of the reaction mixture EtOH:H_2O (60:40) Table S4 entry 16.

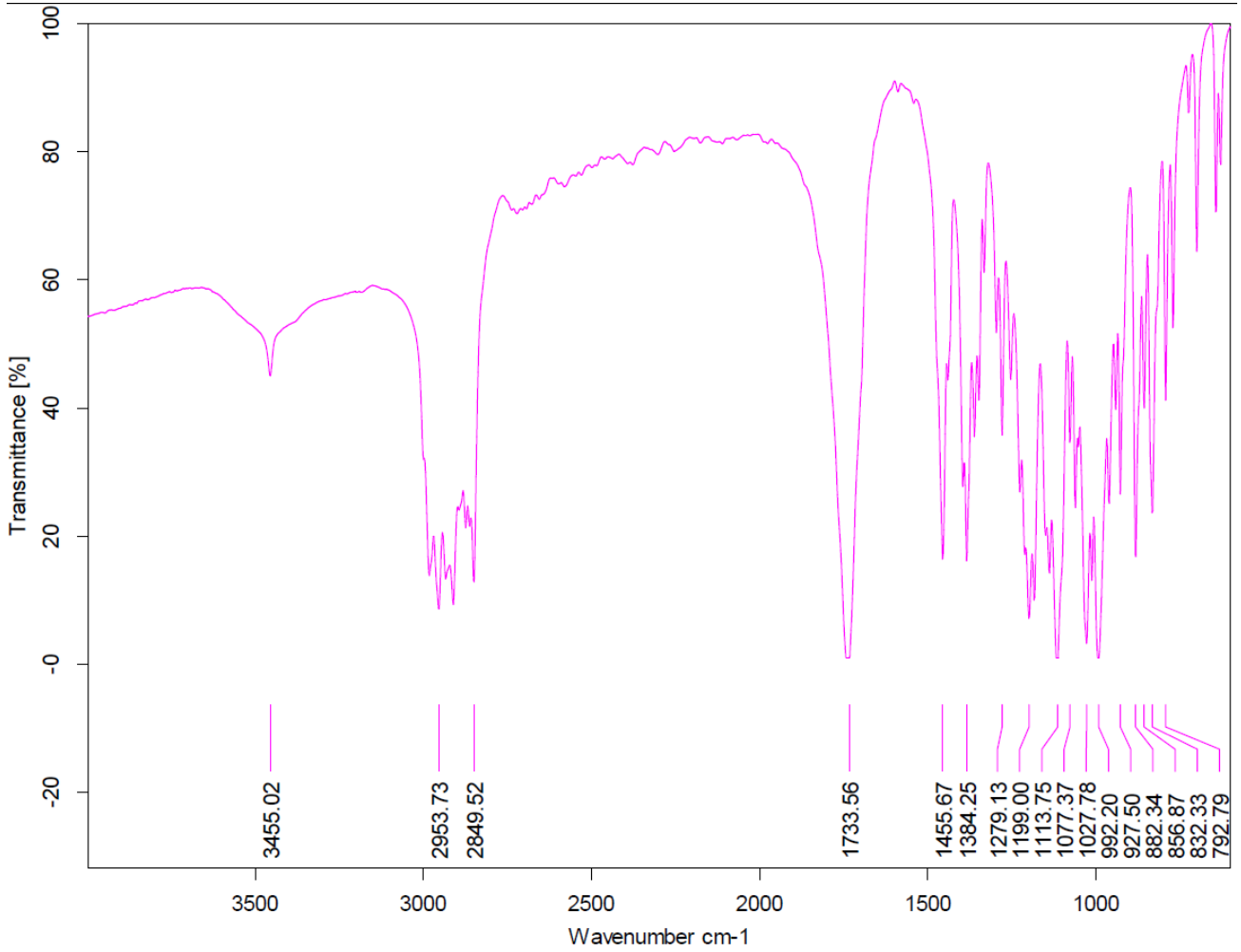

Crude ^{1}H NMR (400 MHz, $CDCl_3$) after removal of volatiles with reaction conditions shown in Table S5, entry 4 (EtOH:H_2O 60:40), following continuous flow photo-oxidation and allowing mixture to stand in air for 24 h. Mesitylene was added as an internal standard (1.0 eq.)

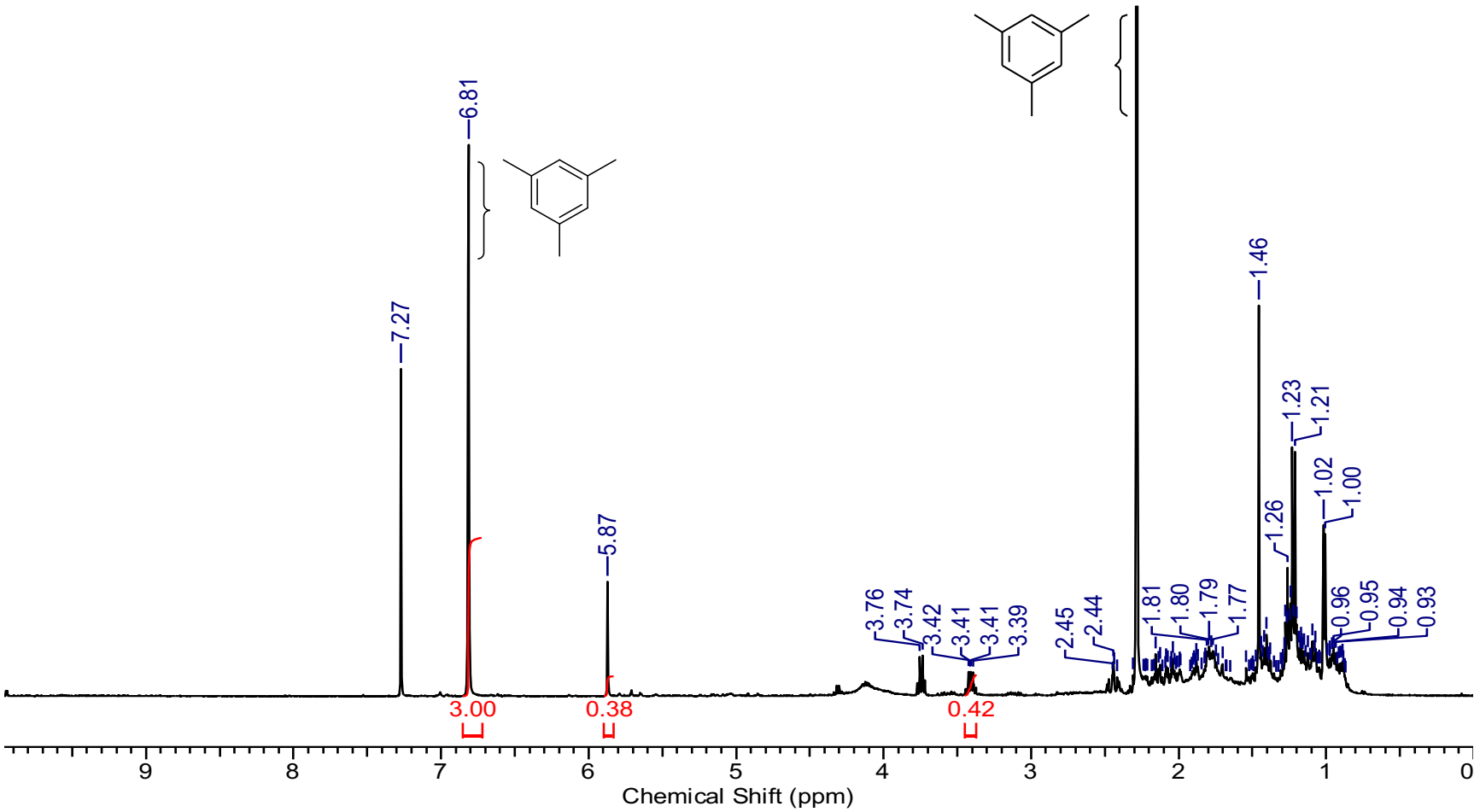

7. Crystal data of artemisinin isolated from Table S4, entry 16

Single crystals of $C_{15}H_{22}O_5$ artemisinin were taken directly from the reaction vessel. A suitable crystal was selected and mounted in fomblin film on a micromount on a GV1000, Atlas diffractometer. The crystal was kept at 120(2)K during data collection. Using Olex2,[43] the structure was solved with the olex2.solve[44] structure solution program using Charge Flipping and refined with the ShelXL[45] refinement package using Least Squares minimization.

Crystal structure determination of artemisinin

Crystal Data for $C_{15}H_{22}O_5$ (M =282.32): orthorhombic, space group $P2_12_12_1$ (no. 19), a = 6.32081(9) Å, b = 9.31057(18) Å, c = 23.9696(4) Å, V = 1410.62(4) Å^3, Z = 4, T = 120(2) K, μ(CuKα) = 0.817 mm^{-1}, *Dcalc* = 1.329 g/mm^3, 35814 reflections measured (7.376 ≤ 2Θ ≤ 152.53), 2925 unique (R_{int} = 0.0317, R_{sigma} = 0.0119) which were used in all calculations. The final R_1 was 0.0252 (I > 2σ(I)) and wR_2 was 0.0668 (all data). Absolute structure parameter -0.01(3).

Structure of artemisinin, as determined by single crystal X-ray diffraction.

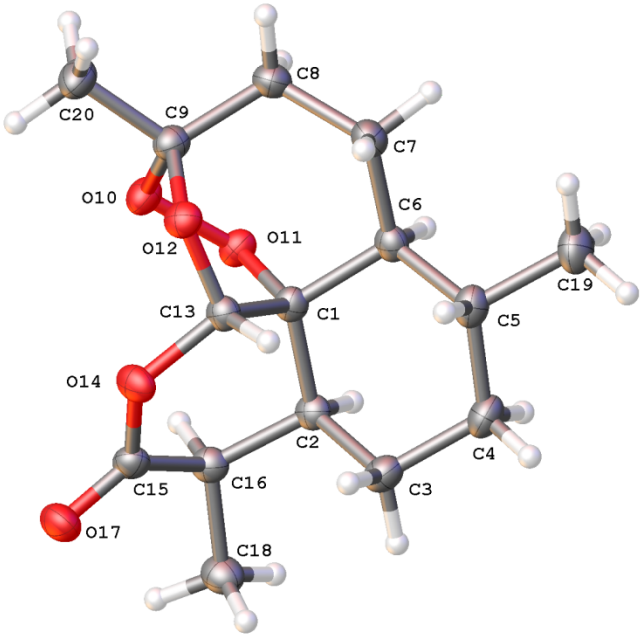

Le Bail fitting of the single crystal structure of 1 against the bulk phase of 1. The final R_{wp} was 8.791.

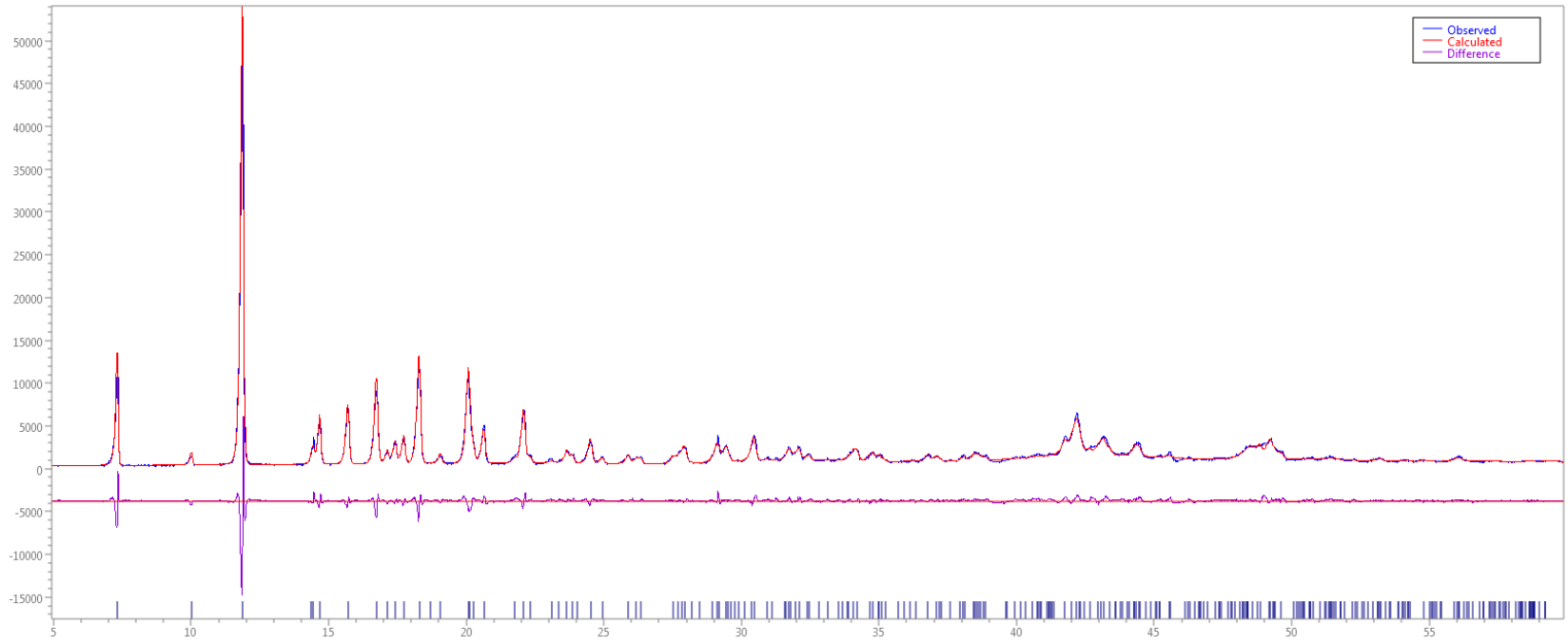

Le Bail fitting of the single crystal structure of 1 against a commercial sample of artemisinin. The final R_{wp} was 9.610.

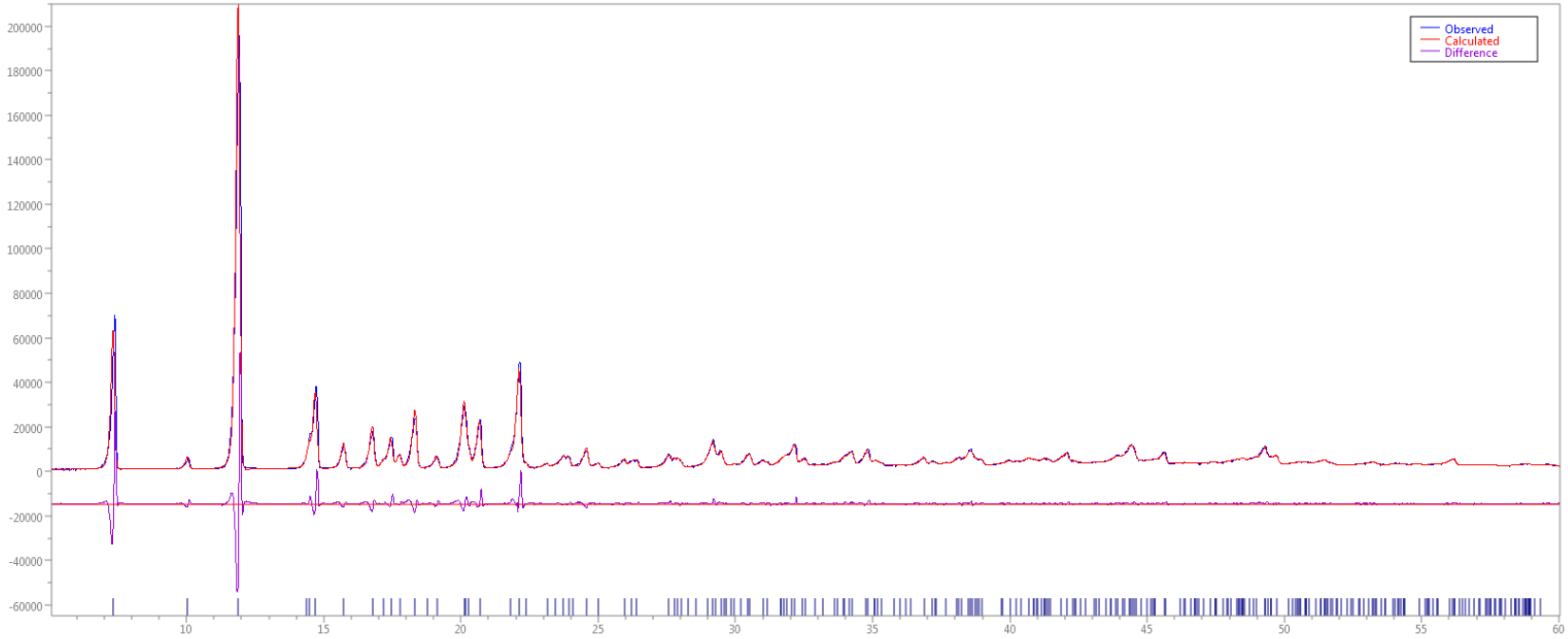

8. Analysis of impurities from reaction mixture table S4, entry 16

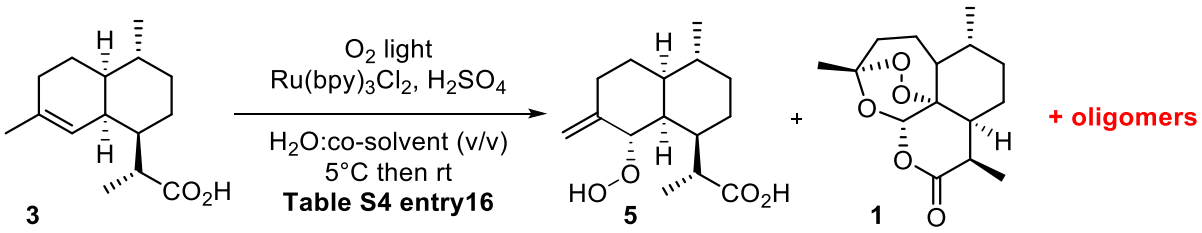

Scheme S10: reaction scheme showing the major products and remaining impurities obtained from conditions described in Table S4, entry 16.

Our model studies described earlier in table S4 showed no products other than **1** and **5** distinguishable by NMR analysis with yields approximating 50% and 10% respectively. Therefore we carried out a full purification of a batch experiment (Table S4, entry 16) which allowed to isolate **1** and the stable minor hydroperoxide isomer **5** by crystallization and column chromatography (silica gel, cyclohexane:EtOAc, 90:10). The same column chromatography was then flushed with pure EtOAc and then EtOH to afford a light yellow oily residue after removal of the volatiles, the characterization of which was not possible by ^{1}H and ^{13}C NMR analysis and was further assigned as an oligomeric compound by MALDI analysis (see below).

MALDI analysis, fraction 1 (EtOAc): positive detection, m/z (100) 1212.998

DCTB 30% Laser

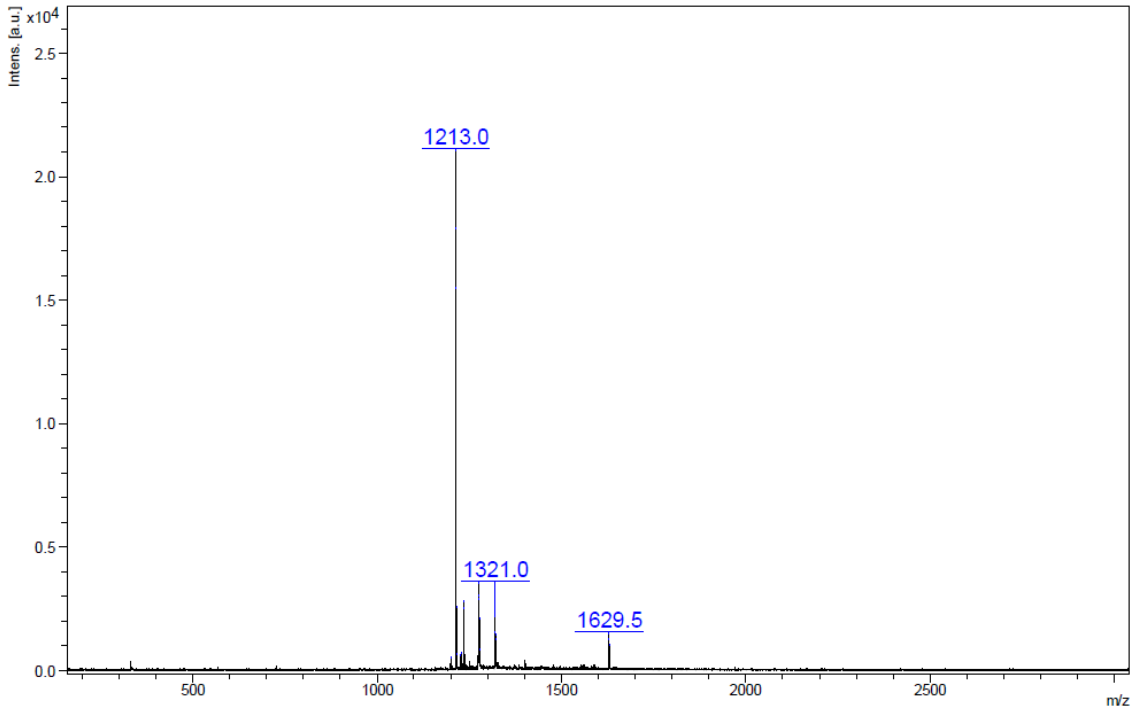

MALDI analysis, fraction 2 (EtOH): positive detection, m/z (100) 1213.344

DCTB 50% Laser

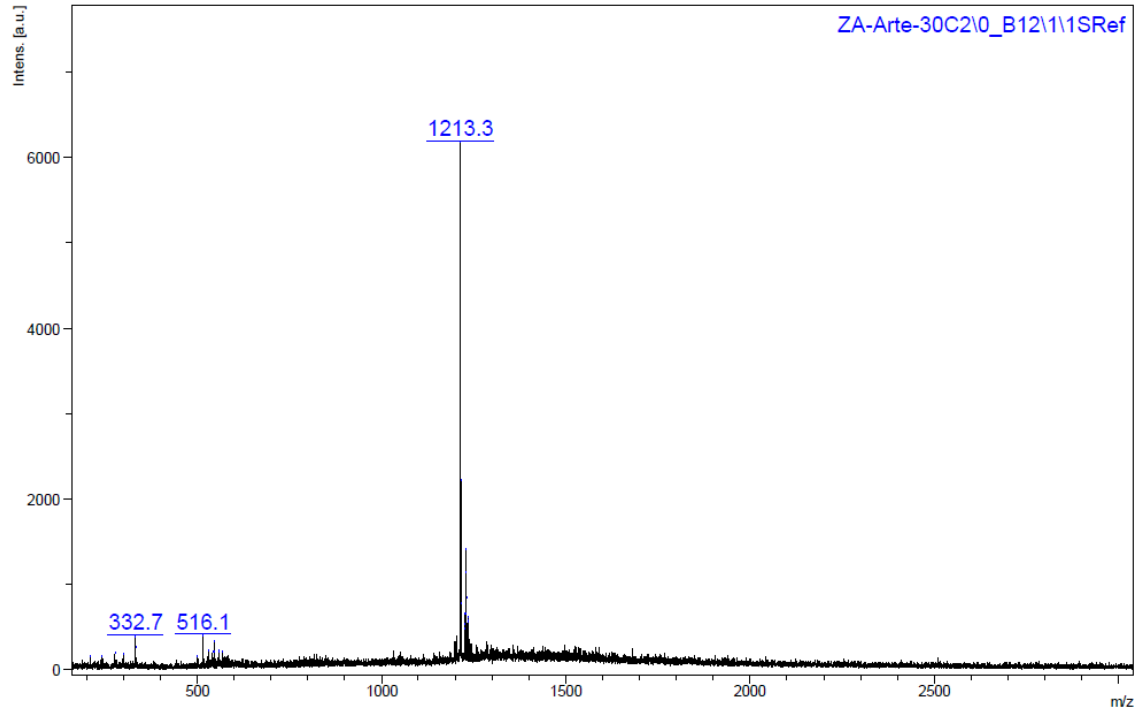

^{1}H NMR experiment (C_6D_6, 300MHz) to attempt dissection of the reaction cascade and trapping of intermediate 6 before second oxidation with $^3O_2$ occurs:

Based on the preceding experimental results from Sy and Brown,[15] it was possible to trap compound **6** in the presence of an internal standard (biphenyl, 0.1 eq.) and to measure the selectivity after the Hock cleavage step (**4** to **6**) before oxidation to **1**. The experiment was carried out as described below in THF as the reaction solvent and was monitored by ^{1}H NMR in C_6D_6 after careful degas and evaporation of the volatiles.

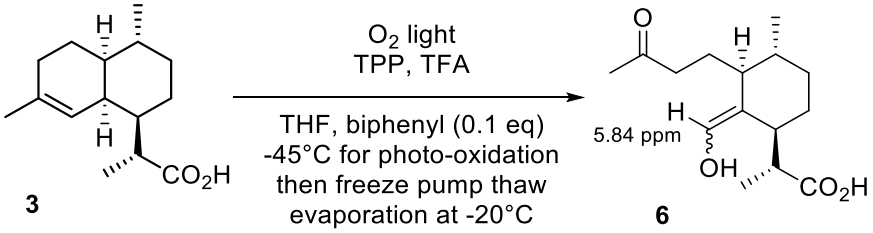

Scheme S11: One pot trapping experiment of Hock cleavage product **6** from **3**

In a 2 necked round bottom flask, **3** (500 mg, 2.12 mmol), TPP (2 mg, 0.003 mmol) and biphenyl (32.7 mg, 0.212 mmol) are dissolved in 25 mL of THF. The reaction mixture is cooled to -45 ºC using a acetonitrile dry-ice cooling bath. The solution is oxygenated by continuous bubbling of O_2 at atmospheric pressure with LED irradiation for 2.5 hours. The conversion and selectivity to the desired product **6** are monitored by ^{1}H NMR by taking regular aliquots concentrated under high vacuum. Oxygen bubbling was ceased and the mixture was degassed by freeze pump thaw and dried by evaporation of the volatiles at -20 ºC. Final yield of **6** is measured by integration against internal standard by ^{1}H NMR (C_6D_6, 300MHz)

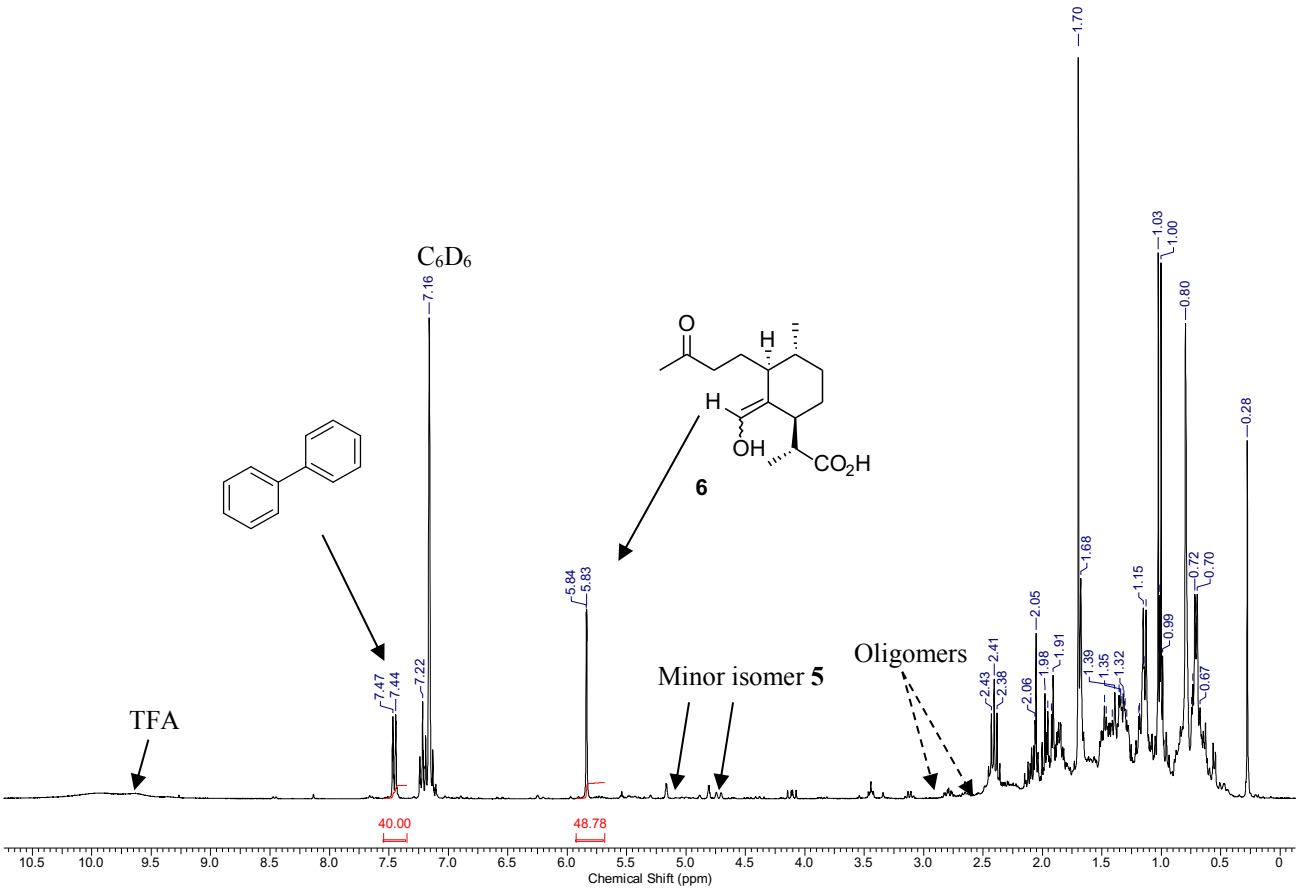

Figure S10: Selectivity before triplet oxygen oxygenation

As mentioned in the literature, enol **6** is a relatively unstable compound that reacts with O_2 to produce **1**. Existence of **6** has been proved and assigned by Sy and Brown in $CDCl_3$[15] and several competitive pathways have been proposed to occur once **6** is formed. We provide further evidence that the formation of oligomers can occur before the formation of **6** which in our hands turned to be stable at room temperature in C_6D_6 and in solvent free conditions at -10 ºC. We found that **6** only reacted when subjected to air to form **1**. The step from **6** to **1** was shown to be quantitative. Even if the selectivity measured at that stage corresponds to the one observed in the experimental conditions from **3** to **1**, more in depth studies in deuterated solvents should help to ascertain the fact that loss of material occur during the formation of **6** (Scheme S10).

Scheme S12: Proposal for the formation oligomeric side products from peroxide **4**.

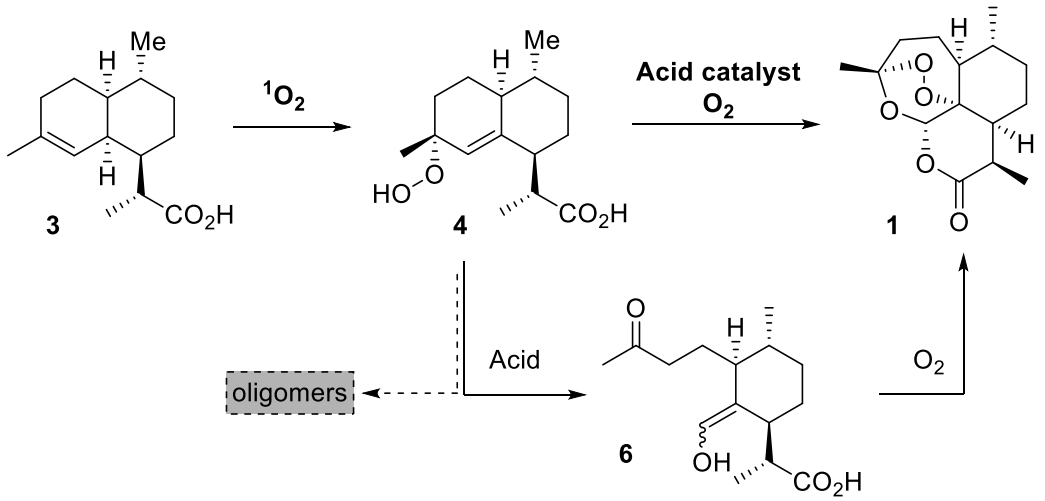

Additional References

43. Dolomanov, O.V., Bourhis, L.J., Gildea, R.J, Howard, J.A.K. & Puschmann, H. (2009), J. Appl. Cryst. 42, 339-341.

44. Bourhis, L.J., Dolomanov, O.V., Gildea, R.J., Howard, J.A.K., Puschmann, H. (2013). in preparation

45. Sheldrick, G.M. (2008). Acta Cryst. A64, 112-122